VAL genes regulate vegetative phase change via miR156-dependent and independent mechanisms

Jim P. Fouracre[1], Jia He[1,3], Victoria J. Chen[1], Simone Sidoli[2] and R. Scott Poethig[1]*

[1] Biology Department, University of Pennsylvania, Philadelphia, Pennsylvania, 19104, USA

[2] Department of Biochemistry, Albert Einstein College of Medicine, Bronx, New York 10461, USA

[3]Current address: Cold Spring Harbor Laboratory, Cold Spring Harbor, New York 11724, USA

* Corresponding author: Poethig, R. S. (spoethig@sas.upenn.edu)

Summary

How organisms control when to transition between different stages of development is a key question in biology. In plants, epigenetic silencing by Polycomb repressive complex 1 (PRC1) and PRC2 plays a crucial role in promoting developmental transitions, including from juvenile-to-adult phases of vegetative growth. It is well established that PRC1/2 repress the master regulator of vegetative phase change, miR156, leading to the transition to adult growth, but how this process in temporally regulated is unknown. Here we investigate whether transcription factors in the *VIVIPAROUS/ABI3-LIKE* (*VAL*) gene family provide the temporal signal for the epigenetic repression of miR156. Exploiting a novel *val1* allele, we found that *VAL1* and *VAL2* redundantly regulate vegetative phase change by controlling the overall level, rather than temporal dynamics, of miR156 expression. Furthermore, we discovered that *VAL1* and *VAL2* also act independently of miR156 to control this important developmental transition.

Keywords

Developmental transitions; vegetative phase change; miR156; *SPL*; *VAL1*; epigenetic silencing

Introduction

Flowering plant development is underpinned by transitions between stereotypical stages of growth: embryogenesis, seed maturation, juvenile and adult phases of vegetative development and flowering (Huijser and Schmid, 2011). The correct timing of these transitions is critical to plant survival and, ultimately, reproductive success. Vegetative phase change describes the transition from juvenile-to-adult vegetative growth and is associated with changes to multiple traits, including leaf morphology, light-use efficiency, herbivore resistance and shoot physiology (Gou et al., 2011; Lawrence et al., 2020; Leichty and Poethig, 2019; Mao et al., 2017). In *Arabidopsis thaliana*, the juvenile phase is characterized by small round leaves that lack both trichomes on the abaxial surface and serrations. Adult leaves, on the other hand, are larger, more elongated, serrated and produce abaxial trichomes (Telfer et al., 1997).

Vegetative phase change is triggered by activity of members of the *SQUAMOSA PROMOTER BINDING PROTEIN-LIKE* (*SPL*) family of transcription factors, which are post-transcriptionally repressed during juvenile development by the microRNAs miR156/miR157 (Fouracre and Poethig, 2019; Wu and Poethig, 2006; Wu et al., 2009; Xu et al., 2016a). miR156/miR157 are encoded by multiple genes of which *MIR156A* and *MIR156C* are the most functionally significant (He et al., 2018). The expression of *MIR156A* and *MIR156C* declines during juvenile growth (Yang et al., 2013b; Yu et al., 2013), leading to the de-repression of their *SPL* targets and the transition to adult growth. Elucidating what controls the decline in *MIR156A*/*C* expression is therefore critical to understanding how the juvenile-to-adult transition is regulated in plants.

67 The molecular mechanisms that lead to the temporal repression of *MIR156A/C*
68 are only beginning to be understood. The activity of Polycomb Group (PcG)
69 transcriptional repressors appears critical. There are two functional complexes of PcG
70 proteins in plants, both of which repress gene expression through covalent histone
71 modifications. PcG repressive complex 1 (PRC1) consists of a H2A E3 ubiquitin ligase
72 module containing one AtBMI1 protein (AtBMI1A/B/C) and one AtRING1 protein
73 (RING1A/B). PRC1 represses gene expression through ubiquitination of H2A
74 (H2AK119ub) (Bratzel et al., 2010; Calonje, 2014; Yang et al., 2013a). The PRC2
75 complex includes histone methyltransferases such as *CURLY LEAF* (*CLF*) and
76 *SWINGER* (*SWN*) and promotes H3 trimethylation (H3K27me3) (Chanvivattana et al.,
77 2004; Goodrich et al., 1997).
78 We have previously found that H3K27me3 increases at *MIR156A/C* in a PRC2-
79 dependent manner during juvenile development, and that vegetative phase change is
80 delayed in *swn* mutants (Xu et al., 2016b). The temporal deposition of H3K27me3 is
81 accompanied by depletion of the antagonistic H3K27ac mark that is associated with
82 active transcription. miR156 accumulation is also repressed by PRC1, as *atbmi1a/b*
83 mutants exhibit delayed vegetative phase change (Pico et al., 2015). In addition, we
84 have found that accumulation of the active histone mark H3K4me3 decreases at
85 *MIR156A/C* during vegetative development (Xu et al., 2018).
86 The findings that H3K27me3 replaces H3K27ac and H3K4me3 at *MIR156A/C*
87 over time, and that PRC1/PRC2-activity promotes vegetative phase change, led us to
88 propose that the temporal dynamics of miR156 accumulation are coordinated by
89 antagonistic patterns of active (H3K27ac, H3K4me3) and repressive (H3K27me3)

90 histone modifications (Xu et al., 2018, 2016b). In this model the stochastic removal of
91 H3K27ac/H3K4me3 facilitates the deposition of H3K27me3 and the gradual epigenetic
92 silencing of miR156. Similar mechanisms have been reported to function at other
93 developmental transitions (Yang et al., 2014). For example, during flowering, H3K27
94 deacetylation is a pre-requisite for PRC2-mediated H3K27me3 deposition at
95 *FLOWERING LOCUS C* (*FLC*) (Zeng et al., 2020), and during seed maturation, PRC1
96 promotes the exchange of H3K4me3 for H3K27me3 at *DELAY OF GERMINATION1*
97 (*DOG1*) and *ABSCISIC ACID INSENSITIVE3* (*ABI3*) (Molitor et al., 2014).
98 Although there is good evidence that *MIR156A/C* are epigenetically silenced
99 during vegetative development, how this mechanism is regulated temporally remains
100 unknown. *VIVIPAROUS/ABI3-LIKE* (*VAL*) genes are excellent candidates for temporal
101 effectors in this model. *VAL* genes encode B3 domain transcription factors that are
102 closely related to the *ABI3/FUSCA3* (*FUS3*)/*LEAFY COYTLEDON2* (*LEC2*) clade of
103 embryogenesis regulators. There are three *VAL* genes in *Arabidopsis*, of which *VAL1*
104 and *VAL2* (also known as *HSI2* and *HSL2* respectively) are the most functionally
105 important (Suzuki et al., 2007). VAL proteins repress their targets by binding to 6 base
106 pair RY-sequence motifs (CATGCA) via their B3 domain (Chen et al., 2018, 2020; Guo
107 et al., 2013; Jing et al., 2019; Qüesta et al., 2016; Suzuki et al., 1997; Yuan et al.,
108 2016).
109 A number of observations suggest that *VAL* genes might provide the temporal
110 information that coordinates vegetative phase change: 1) *VAL* genes regulate other
111 developmental transitions, i.e. seed maturation (Suzuki et al., 2007; Yang et al., 2013a)
112 and flowering (Qüesta et al., 2016; Yuan et al., 2016); 2) *MIR156A/C* expression is

113 elevated in *val1/2* mutants (Pico et al., 2015); 3) VAL1/2 physically interact with several
114 histone deacetylases (*HDA6/9/19*) (Chhun et al., 2016; Qüesta et al., 2016; Zeng et al.,
115 2020; Zhou et al., 2013); and 4) *VAL* genes promote PRC1 and PRC2-binding (Chen et
116 al., 2018; Pico et al., 2015; Qüesta et al., 2016; Yuan et al., 2020, 2016)

117 In this study we investigated whether *VAL* genes function as temporal regulators
118 of vegetative phase change. We report that reduced *VAL* activity significantly delays the
119 timing of vegetative phase change through both miR156-dependent and independent
120 mechanisms. We find that the temporal decline in miR156 expression is remarkably
121 robust and is insensitive to loss of *VAL* function, inhibition of VAL1-binding and the
122 combined loss of *VAL1* and PRC2 components. Finally, we show that the effects of
123 *VAL1* on the timing of vegetative phase cannot be explained by temporal changes in its
124 interactions with other proteins.

125

126 **Results**

127 ***VAL* genes promote vegetative phase change**

128 To investigate the role of *VAL* genes in vegetative phase change, we exploited a novel
129 mutant we identified in an EMS screen for plants exhibiting prolonged juvenile
130 development. Mapping-by-sequencing revealed a substitution at the *VAL1* locus,
131 resulting in the conversion of a highly conserved arginine residue to a cysteine in the N-
132 arm of the VAL1 B3 DNA-binding domain (Figure S1A). This arginine residue is critical
133 for VAL1 binding to target RY-motifs (Sasnauskas et al., 2018). The mutation in *VAL1*
134 was confirmed to be the cause of the late juvenile phenotype by its failure to
135 complement the null *val1-2* T-DNA insertion allele, and by the ability of the *VAL1*

136 genomic sequence to rescue this phenotype (Figure S1B,C). Unlike *val1-2*, the novel
137 *val1* allele is semi-dominant, and delays vegetative phase change when heterozygous
138 (Figure S1D). We therefore named this new allele *val1-5(sd)*, consistent with the
139 nomenclature of existing *val1* alleles (Veerappan et al., 2012).

140 Both *val1-5(sd)* and *val1-2* exhibit delayed vegetative phase change, with *val1-*
141 *5(sd)* having a stronger effect on the timing of abaxial trichome production than *val1-2*
142 (Figure S1B). As *VAL1* functions redundantly with *VAL2* to regulate other
143 developmental transitions (Qüesta et al., 2016; Suzuki et al., 2007; Tsukagoshi et al.,
144 2007; Yuan et al., 2016), we tested the effects of *val1; val2* double mutants on
145 vegetative phase change. Previous analyses of *VAL* gene function have utilized *val1-2;*
146 *val2-1* and *val1-2; val2-3* double mutants. However, seedling development is so strongly
147 perturbed in *val1-2; val2-1* and *val1-2; val2-3* plants (Suzuki et al., 2007; Tsukagoshi et
148 al., 2007; Yang et al., 2013a; Yuan et al., 2020) that analyses of vegetative growth is
149 problematic in these backgrounds. Therefore, we generated new *val1; val2*
150 combinations using *val2-3* and a previously uncharacterized T-DNA insertion allele we
151 named *val2-4* (Figure 1A). Consistent with previous studies (Suzuki et al., 2007;
152 Tsukagoshi et al., 2007; Yuan et al., 2016), *val2* single mutants had no discernible
153 effect on vegetative phase change (Figure 1B, S1E). However, loss of *VAL2* activity
154 enhanced the phenotypes of *val1-2* and *val1-5(sd)*. *val1-2; val2-4* and *val1-5(sd); val2-3*
155 both exhibited delayed abaxial trichome production relative to *val1-2* and *val1-5(sd)*,
156 respectively (Figure 1C). *val1-5(sd)*; *val2-3* flowered significantly later than *val1-5(sd)*
157 (Figure 1D) and *val1-2; val2-4* produced leaves that were significantly more juvenile in
158 shape (i.e. rounder) than *val1-2* (Figure 1E). Neither double mutant combination was as

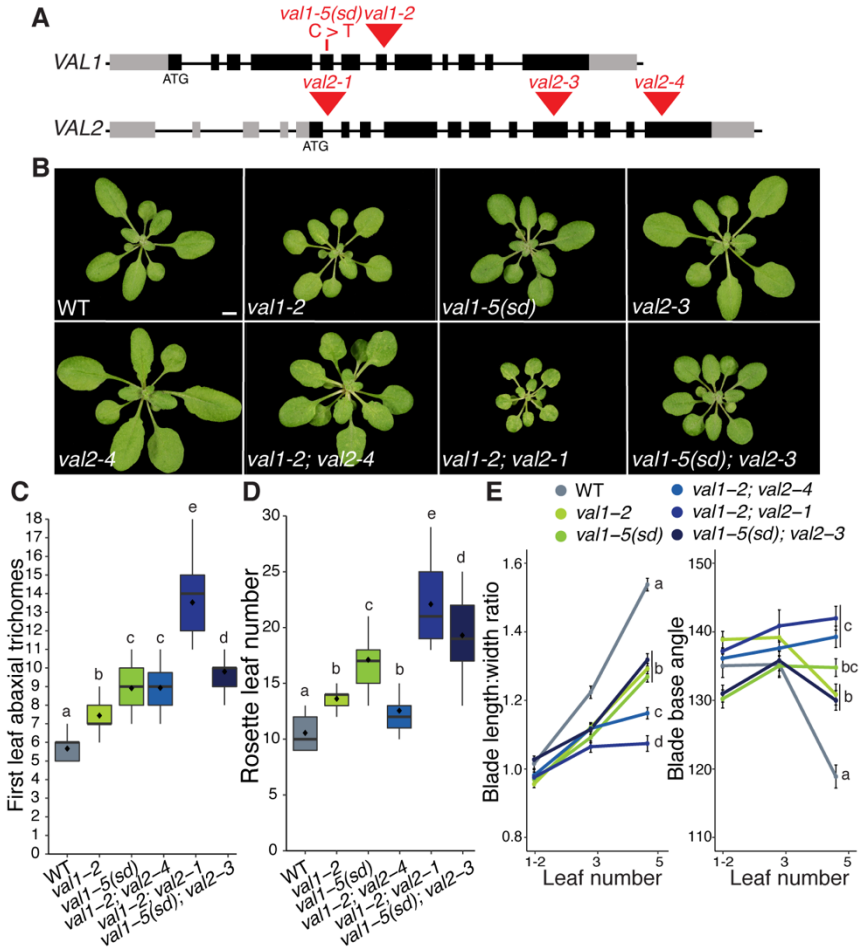

Figure 1. *VAL* genes redundantly regulate vegetative phase change

(A) Schematic of *val1* and *val2* alleles used in this study – grey boxes represent UTRs, black boxes represent exons, red triangles represent T-DNA insertions, red line represents EMS-induced base substitution.

(B) Phenotypes at 21 DAG in LD conditions, scale bar = 5mm.

(C-E) Quantitative analysis of vegetative development. Statistically distinct genotypes were identified by one-way ANOVA with *post hoc* Tukey multiple comparison test (letters indicate statistically distinct groups $P < 0.05$; for (E) comparisons were made at leaf 5), all plants grown in LD. (C,D) Boxes display the interquartile range (IQR) (boxes), median (lines) and values beyond 1.5*IQR (whiskers); mean values are marked by ◆. (E) Colored lines represent the mean and black bars the SEM. Sample sizes (C, D) 21-46, (E) 13-46.

173 phenotypically severe as *val1-2; val2-1* (Figure 1C-E). The weaker phenotype of *val1-*
174 *5(sd); val2-3* than *val1-2; val2-3* (Yang et al., 2013a; Yuan et al., 2020) suggests that
175 the semi-dominant phenotype of *val1-5(sd)* is mediated by interaction with *VAL2*.
176 Importantly, the rate of germination was higher in *val1-2; val2-4* and *val1-5(sd); val2-3*
177 relative to existing *val1; val2* double mutants. *val1-2; val2-4* and *val1-5(sd); val2-3* thus
178 provide a balance between phenotypic strength and experimental viability and are
179 useful tools for investigating the role of *VAL* genes in developmental timing.
180

181 **_VAL_ genes function predominantly as quantitative – rather than temporal –**
182 **regulators of miR156 expression**

183 Vegetative phase change results from a temporal decline in miR156 expression (Wu
184 and Poethig, 2006). A previous analysis of *val1-2; val2-1* revealed elevated expression
185 of *MIR156A/C* at a single time point (Pico et al., 2015). To determine whether the delay
186 in vegetative phase change we observed in *val* mutants is associated with a general
187 increase in the level of miR156, or with a delay in the decline in this miRNA, we
188 quantified miR156 expression in the shoot apex and in isolated leaf primordia at
189 different times in shoot development. The primary transcripts of *MIR156A* and *MIR156C*
190 were expressed at similar levels, and exhibited a similar temporal expression pattern, in
191 wild type, *val1-5(sd)* (Figure 2A,B) and *val1-2* shoot apices and leaf primordia (Figure
192 S2). However, the abundance of the mature miR156 miRNA transcript was significantly
193 higher in *val1-5(sd)* leaf primordia than in wild type (Figure 2B), and it was also
194 marginally higher in *val1-5(sd)* shoot apices than in wild type (Figure 2A). The *val1-*
195 *5(sd); val2-3* (Figure 2A,B) and *val1-2; val2-1* (Figure S2) double mutants had stronger

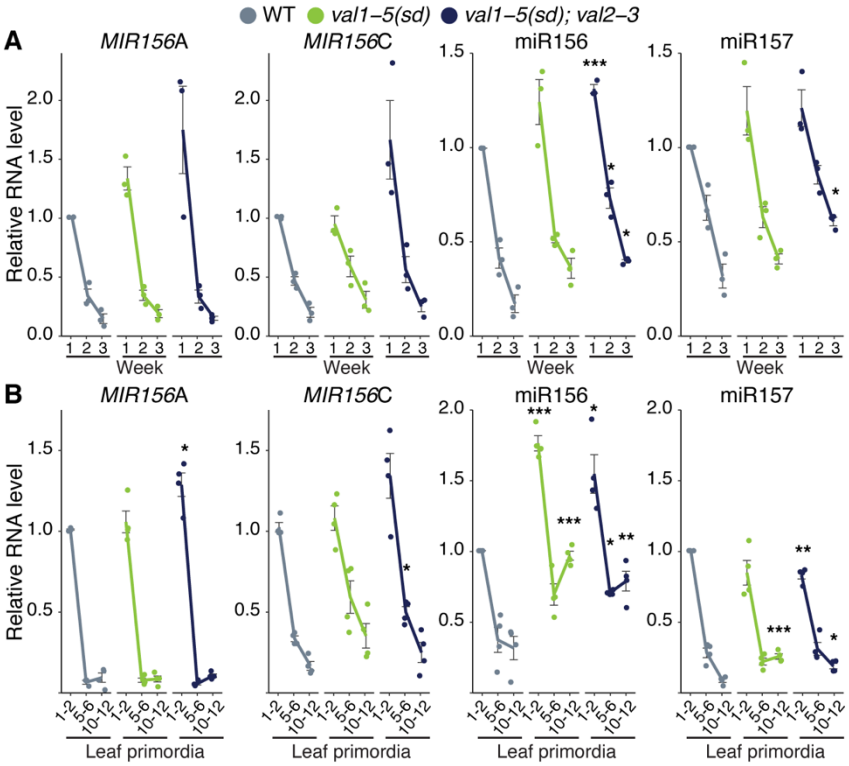

Figure 2. *VAL* genes function predominantly as quantitative regulators of miR156 expression

(A, B) qRT-PCR analyses of gene expression. (A) Shoot apices with leaf primordia (LP) ≥ 1mm removed at 1, 2 and 3 weeks. (B) Isolated LP 0.5-1mm in size. All plants were grown in SD conditions. Each data point represents a biological replicate and is the average of three technical replicates. Coloured lines represent the mean and black bars mean±s.e.m. Asterisks represent significant differences between WT and *val* mutants at the same time point, calculated by an unpaired two-tailed *t*-test with a Bonferroni correction for multiple comparisons (* $P < 0.025$; ** $P < 0.005$; *** $P < 0.0005$).

208 effects on *MIR156A* and *MIR156C* expression than the respective *val1* single mutants,
209 suggesting that *VAL1* and *VAL2* function redundantly to repress *MIR156A* and
210 *MIR156C* transcription. Mature miR156 was elevated throughout development in both
211 the shoot apices (Figure 2A) and the leaf primordia (Figure 2B) of *val1-5(sd); val2-3*
212 double mutants. Loss of *VAL* activity also produced a slight increase in miR157 levels
213 (Figure 2A,B, S2). Although *val1-5(sd); val2-3* increased the abundance of
214 miR156/miR157, it had only a minor effect on the temporal expression patterns of these
215 miRNAs. For example, miR156 expression decreased 2.36-fold between 1W and 2W
216 and 2.31-fold between 2W and 3W in wild type plants, but decreased 1.77 and 1.82-fold
217 between the same time points in *val1-5(sd); val2-3* plants (Figure 2A). Taken together,
218 these data suggest that *VAL* genes function primarily as general, rather than temporal,
219 regulators of miR156 expression.
220

221 **_VAL_ genes coordinate PRC1 and PRC2 recruitment at _MIR156_ loci**

222 We have previously demonstrated that the temporal decline in *MIR156A* and *MIR156C*
223 expression is associated with PRC2-dependent and progressive deposition of
224 H3K27me3 at these loci (Xu et al., 2016b). To determine if *VAL* genes contribute to this
225 process, we examined PRC2 activity in the *val1-5(sd); val2-3* double mutant. As
226 previously reported (Xu et al., 2016b), H3K27me3 levels increased at the *MIR156A* and
227 *MIR156C* loci during vegetative development in wild type plants (Figure 3A,B). Although
228 there was no difference in the temporal pattern of H3K27me3 deposition at *MIR156A* in
229 *val1-5(sd); val2-3*, the rate of H3K27me3 deposition at *MIR156C* was significantly
230 slower in this double mutant (Figure 3B). These results are consistent with a recent

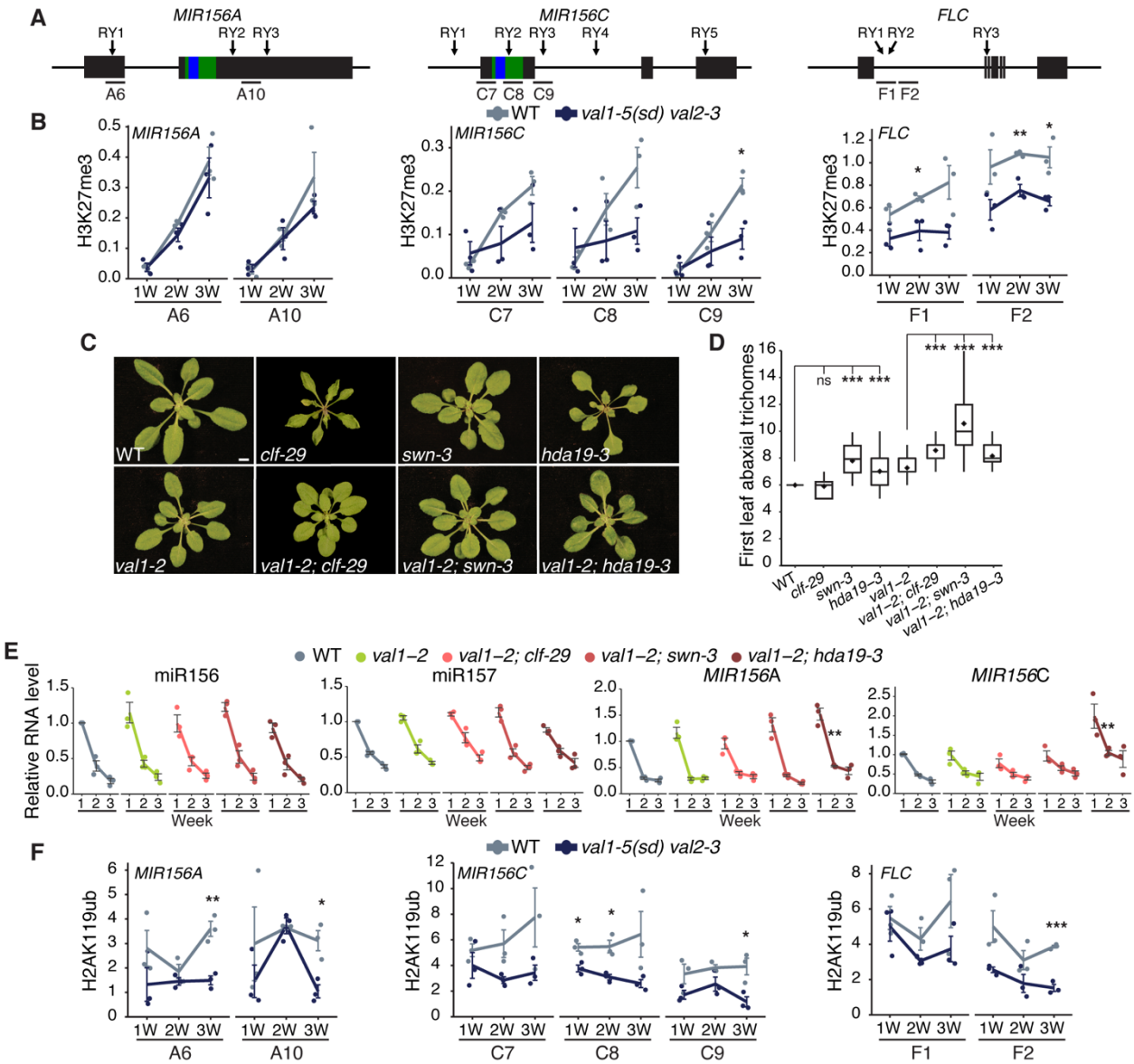

Figure 3. *VAL* genes regulate miR156 activity via-PRC2 and PRC1

(A) Schematics of the primer locations used for ChIP-qPCR. Blue and green bars represent sequences encoding the mature miRNA and miRNA hairpin respectively.

(B) Temporal analysis of H3K27me3 by ChIP-qPCR. Each data point represents a biological replicate and is the average of three technical replicates. Lines represent the mean, bars represent the mean±s.e.m., asterisks represent significant differences between WT and *val1-5(sd); val2-3* at the same time point, calculated by an unpaired two-tailed *t*-test (* $P < 0.05$; ** $P < 0.01$; *** $P < 0.001$). H3K2me3 values are relative to H3 and normalised to *STM* as an internal control. Plants were grown in SD conditions.

(C, D) Phenotypes in LD. (D) Photographs taken at 21DAG, scale bar = 5mm. (E) Asterisks represent significant differences to either WT or *val1-2*, calculated by unpaired two-tailed *t*-test with Bonferroni correction for multiple comparisons (*** $P < 0.00033$). Sample size 22-46.

(E) qRT-PCR analyses of gene expression in shoot apices with LP ≥ 1mm removed at 1, 2 and 3 weeks. Each data point represents a biological replicated and is the average of three technical replicates. Coloured lines represent the mean and black bars represent the mean±s.e.m. Asterisks represent significant differences between *val1-2* and *val1-2; clf-29/val1-2; swn-3/val1-2; hda19-3* at the same time point, calculated by unpaired two-tailed *t*-test with Bonferroni correction for multiple comparisons (** $P < 0.0033$). Plants were grown in SD conditions.

(F) Temporal analysis of H2AK119ub by ChIP-qPCR, values are relative to input and normalised to *ACT7* as an internal control. See (B) for details.

258 genome-wide study that revealed a decrease in H3K27me3 levels at *MIR156C*, but not
259 *MIR156A*, in *val1-2; val2-3* plants (Yuan et al., 2020). As a control, we measured
260 H3K27me3 deposition at the floral regulator *FLC.* In the absence of vernalization, we
261 observed no change in the level of H3K27me3 during vegetative development in wild
262 type plants (Figure 3B). However, consistent with previous reports (Qüesta et al., 2016;
263 Yuan et al., 2016), there was a significant decrease in H3K27me3 at *FLC* in *val1-5(sd);*
264 *val2-3*.

265 *VAL1* is thought to act by recruiting PRC1 which, in turn, promotes the activity of
266 PRC2 (Baile et al., 2020; Calonje, 2014; Zhou et al., 2017). As a genetic test of this
267 hypothesis, we examined the interaction between *val1-2* and *clf-29* and *swn-3,* loss-of-
268 function mutations in the functionally redundant genes that encode the histone
269 methyltransferase activity of PRC2. As we have shown previously (Xu et al., 2016b),
270 *swn-3* had a larger effect on the timing of vegetative phase change than *clf-29* (Figure
271 3C,D). Consistent with the hypothesis that *VAL1* regulates vegetative phase via its
272 effect on PRC2 activity, *clf-29* and *swn-3* interacted synergistically with *val1-2,* in that
273 the double mutants had a much more severe vegetative phase change phenotype than
274 the single mutants (Figure 3C,D). Notably, *val1-2* suppressed the curling leaf phenotype
275 of *clf-29* (Figure 3C), presumably because it enhances *FLC* expression (Lopez-Vernaza
276 et al., 2012). We also examined the interaction between *val1-2* and *hda19-3*, a putative
277 null allele of the histone deacetylase HDA19. *hda19-3* is predicted to delay vegetative
278 phase change because *HDA19* is required for PRC2-mediated repression (Zeng et al.,
279 2020), HDA19 physically interacts with VAL1 (Qüesta et al., 2016) and loss-of *HDA19*
280 enhances H3K4me3 levels (Jang et al., 2011). As predicted, *hda19-3* produced abaxial

281 trichomes significantly later than wild type (Fig. 3D), and *val1-2; hda19-3* double
282 mutants produced abaxial trichomes significantly later than either single mutant.
283 Together, these results suggest that *val* mutations delay vegetative phase change by
284 interfering with the activity of PRC2.

285 To determine whether the synergistic interaction between *clf-29, swn-3, hda19-3*
286 and *val1-2* is due to enhanced miR156/miR157 expression, we quantified expression of
287 the mature miR156 and miR157 miRNAs, and the primary *MIR156A* and *MIR156C*
288 transcripts, in these mutant backgrounds. The overall level and expression pattern of
289 the mature miR156/miR157 transcripts were not affected by *val1-2*, or by *val1-2; clf-29*,
290 *val1-2; swn-3*, and *va1-2; hda19-3* double mutants (Figure 3E). However, *pri-MIR156A*
291 and *pri-MIR156C* transcripts were significantly elevated in *val1-2; hda19-3,* although the
292 rate of decline in the expression of these transcripts was normal. The lack of correlation
293 between the expression of miR156 and the level of *pri-MIR156A* and *pri-MIR156C* is
294 surprising given that these loci are the major sources of miR156. One possibility is that
295 the miRNA processing pathway is compensating for elevated levels of the primary
296 transcripts. In any case, these results suggest that *VAL* genes temporally regulate the
297 deposition of H3K27me3 at specific *MIR156* loci, but are not necessary for the temporal
298 decline in miR156 expression.

299 *VAL* genes also repress gene expression by promoting H2AK119ub deposition
300 via recruitment of PRC1 (Yang et al., 2013a). Unlike H3K27me3 (Figure 3B) (Xu et al.,
301 2016b), we found no evidence that H2AK119ub increases over time at *MIR156A* and
302 *MIR156C* (Figure 3F). However, we did find that *val1-5(sd); val2-3* had significantly
303 lower levels of H2AK119ub than wild type plants. This effect was observed throughout

304 development at *MIR156C*, but seemed to be limited to later in development at
305 *MIR156A*. Importantly, *val1-5(sd); val2-3* had significantly reduced levels of H2AK119ub
306 at *MIR156C* one week after planting, which is before a difference in H3K27me3 is
307 detectable at this locus (Figure 3B). *val1-5(sd); val2-3* also had reduced levels of
308 H2AK119ub at *FLC* (Figure 3F).
309

310 ***VAL1* regulates vegetative phase change via miR156-dependent and miR156-**
311 **independent mechanisms**

312 To investigate whether the effects of *val1-5(sd); val2-3* on the chromatin state of
313 *MIR156A/C* are due to a direct regulatory interaction, we carried out chromatin-
314 immunoprecipitation qPCR using an HA-tagged version of VAL1 (Qüesta et al., 2016).
315 Confirming the results of a recent ChIP-seq study (Yuan et al., 2020), we found VAL1-
316 binding at specific locations within both the *MIR156A* and *MIR156C* loci (Figure 4A,B,
317 S3). The affinity of VAL1 for *MIR156A/C* appeared consistent throughout vegetative
318 development. VAL1/2 bind to RY-sequence motifs, of which there are multiple copies in
319 both *MIR156A* and *MIR156C* (Figure 4A). To determine if these RY-sites are required
320 for the regulation of vegetative phase change, we mutated 5 RY-sites in *MIR156C*
321 individually and in combination. We selected *MIR156C* because it is more sensitive to
322 *VAL* activity than *MIR156A* (Figure 2,3, S2). A C>T substitution that eliminates VAL1
323 binding (Sasnauskas et al., 2018) was introduced in one or all of these sites in a
324 genomic construct of *MIR156C*. Wild type and mutant constructs were then transformed
325 into a *mir156a; mir156c; mir157a; mir157c quadruple mutant* (*qm*) background. We
326 chose this background because endogenous miR156/miR157 activity has been largely

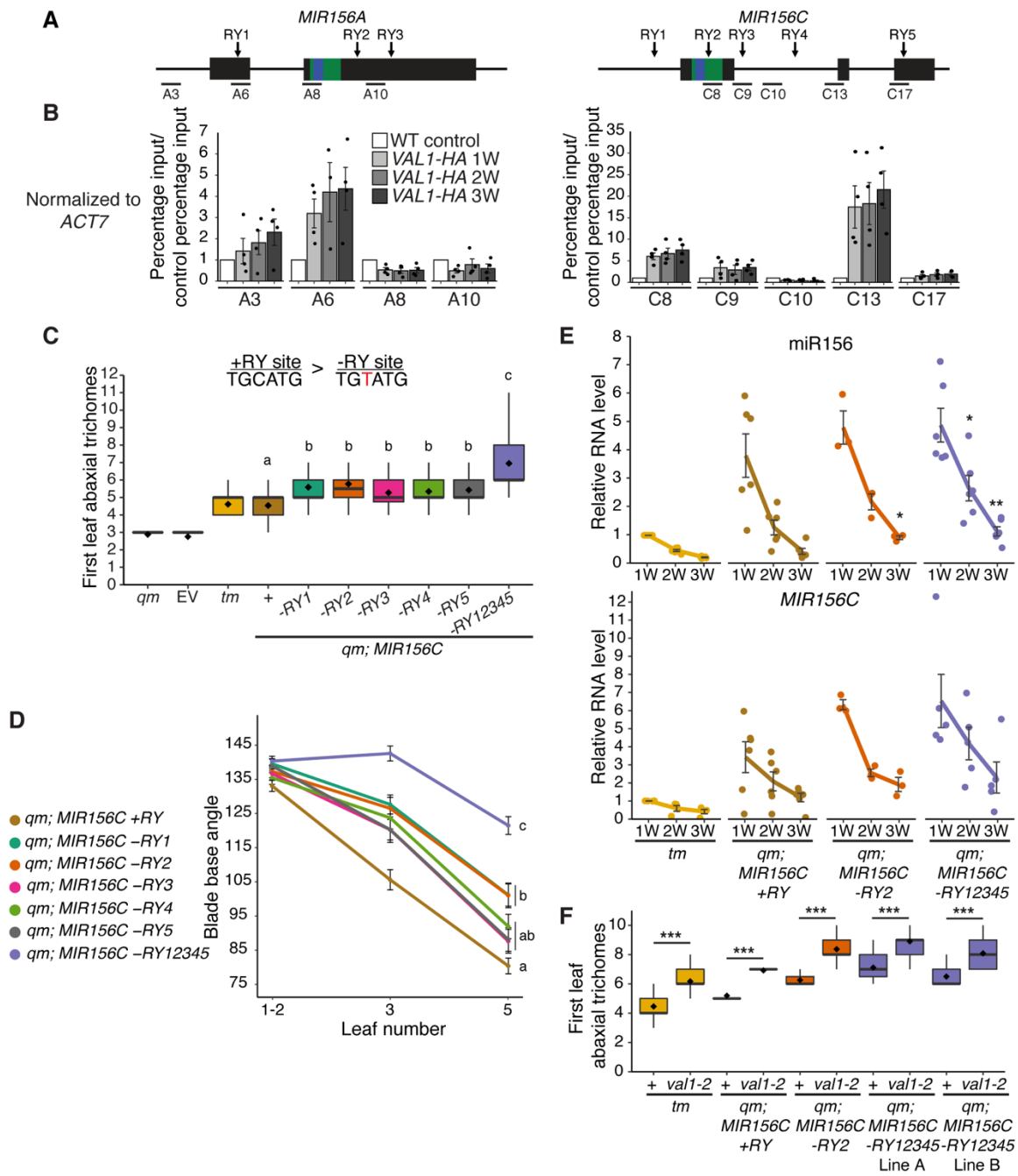

Figure 4. Loss of RY VAL-binding motifs at the *MIR156C* locus delays vegetative phase change

(A) Schematic depicting the location of primers used for ChIP-qPCR, the sequences encoding the miR156 hairpin and mature miRNA are coloured green and blue respectively.

(B) Anti-HA ChIP-qPCR of WT Col control plants at 2W and *VAL1::VAL1-HA; val1-2; FRI-Sf2* plants at 1, 2 and 3W of growth. The data is presented as percentage input normalized to *ACT7* and is displayed relative to WT. Each data point represents a biological replicate and is the average of three technical replicates, bars represent the mean and error bars the mean±s.e.m.

338 (C, D) Phenotypes of T1 plants transformed with *MIR156C* RY variants. Statistically
339 distinct genotypes were identified by one-way ANOVA with *post hoc* Tukey
340 multiple comparison test (letters indicate statistically distinct groups $P < 0.05$;
341 comparison in (C) made at leaf 5). *qm = mir156a mir156c mir157a mir157c*
342 *quadruple mutant, tm = mir156a mir157a mir157c triple mutant,* EV = empty
343 vector. (C) Colored lines represent the mean and black bars the mean±s.e.m.
344 Sample size (B) 26-52, (C) 37-51.
345 (E) qRT-PCR analyses of gene expression in shoot apices with LP ≥ 1mm removed
346 at 1, 2 and 3 weeks. Each data point represents an independent homozygous T3
347 line and is the average of three technical replicates. Colored lines represent the
348 mean and black bars the mean±s.e.m. Asterisks represent significant differences
349 between *qm; MIR156C* and *qm; MIR156C -RY* lines at the same time point,
350 calculated by an unpaired two-tailed *t*-test with a Bonferroni correction for
351 multiple comparisons (* $P < 0.025$, ** $P < 0.005$).
352 (F) Genetic interaction between *val1-2* and *MIR156C* RY deletions. Asterisks
353 represent significant differences between plants with wild type or null *VAL1*
354 alleles calculated by an unpaired two-tailed *t*-test (*** $P < 0.001$). Sample size
355 24-36. Phenotyping analyses were carried out in LD conditions, gene expression
356 and ChIP analyses were carried out in SD conditions.
357

358 eliminated and it is therefore sensitive to small changes in the level of miR156 (He et
359 al., 2018). Plants transformed with a wild type *MIR156C* construct (+*RY*) produced
360 leaves with abaxial trichomes at the same node as the *mir156a; mir157a; mir157c triple*
361 *mutant tm* (Figure 4C). *tm* has an endogenous copy of *MIR156C*, confirming that the
362 transgenic *MIR156C* sequence is fully functional. Deletion of individual RY-sites
363 produced a significant delay in the timing of abaxial trichome production relative to
364 *MIR156C +RY*, and deletion of all 5 RY-sites produced a more significant delay than
365 deletion of any single site (Figure 4C). A similar result was obtained in the case of the
366 angle of the leaf base (Figure 4D). These results demonstrate that all five RY-sites are
367 important for the expression of *MIR156C*, and that they function additively. Individual
368 RY-sites have also been shown to interact additively to repress the VAL1-PRC2 targets
369 *FLC* and *DOG1* (Chen et al., 2020; Yuan et al., 2016).

370 To determine if these phenotypic effects are due to altered *MIR156C* expression,
371 we quantified miR156 levels in *MIR156C +RY, MIR156C -RY2* and *MIR156C -RY12345*
372 plants. *MIR156C -RY2* was selected because it has a marginally stronger effect than
373 other individual -RY deletions (Figure 4C,D). Although there was considerable variation
374 in miR156 levels between independent transgenic lines, *MIR156C -RY2* and *MIR156C -*
375 *RY12345* plants had significantly more miR156 than plants transformed with *MIR156C*
376 *+RY* (Figure 4E, S4). However, the temporal expression pattern of *MIR156C* was
377 identical in -*RY* and +*RY* plants.

378 To establish whether the effects of RY-deletion are *VAL1*-dependent, we crossed
379 *val1-2* into the *qm; MIR156C +/-RY* lines. If the delay in vegetative phase change in
380 *MIR156C -RY* lines is a consequence of reduced VAL1 binding, *val1-2* should have less

381 effect in *MIR156C -RY* lines than in *MIR156C +RY* lines or the *tm*, in which RY sites are
382 intact. Surprisingly, we found that loss-of *VAL1* significantly delayed abaxial trichome
383 production in *MIR156C -RY* as well as *MIR156C +RY* and *tm* plants (Figure 4F). It is
384 possible that *MIR156C* RY-sites are bound by other B3 domain transcription factors.
385 However, RY-binding is restricted to the *ABI3/FUS3/LEC2* and *VAL* clade of B3 domain
386 genes (Kagaya et al., 1999; Sasnauskas et al., 2018; Yuan et al., 2016). The
387 expression of *ABI3/FUS3/LEC2* is largely restricted to seed development (Carbonero et
388 al., 2017) and therefore these genes are unlikely to regulate vegetative shoot identity.
389 Moreover, FUS3 and ABI3 directly promote the expression of *MIR156C* (Tian et al.,
390 2020; Wang and Perry, 2013). A role for these genes in the regulation of *MIR156C* post-
391 germination is thus inconsistent with the juvenilized phenotype and elevated miR156
392 expression we found in *MIR156C -RY* plants. (Figure 4C-E). With regard to the potential
393 effects of other *VAL* genes, we observed no vegetative phase change phenotype in *val2*
394 single mutants (Figure 1B, S1E) and *VAL3* has limited expression and functionality
395 relative to *VAL1* and *VAL2* (Suzuki et al., 2007). Alternatively, this result suggests that
396 *VAL1* may regulate vegetative phase change through both miR156-dependent and
397 miR156-independent mechanisms. This interpretation is supported by the observation
398 that loss-of *VAL1* and PRC2-components strongly delayed vegetative phase change but
399 had only minor effects on miR156 expression (Figure 3C-E).
400 To test this hypothesis, we introgressed *val1-2* into the *qm* genetic background,
401 which has very low levels of miR156/miR157 (He et al., 2018). Although the gross
402 morphology (Figure 5A) of *val1-2*; *qm* seedlings was indistinguishable from that of *qm*
403 plants, *val1-2* partially suppressed the effect of the *qm* genotype on the morphology of

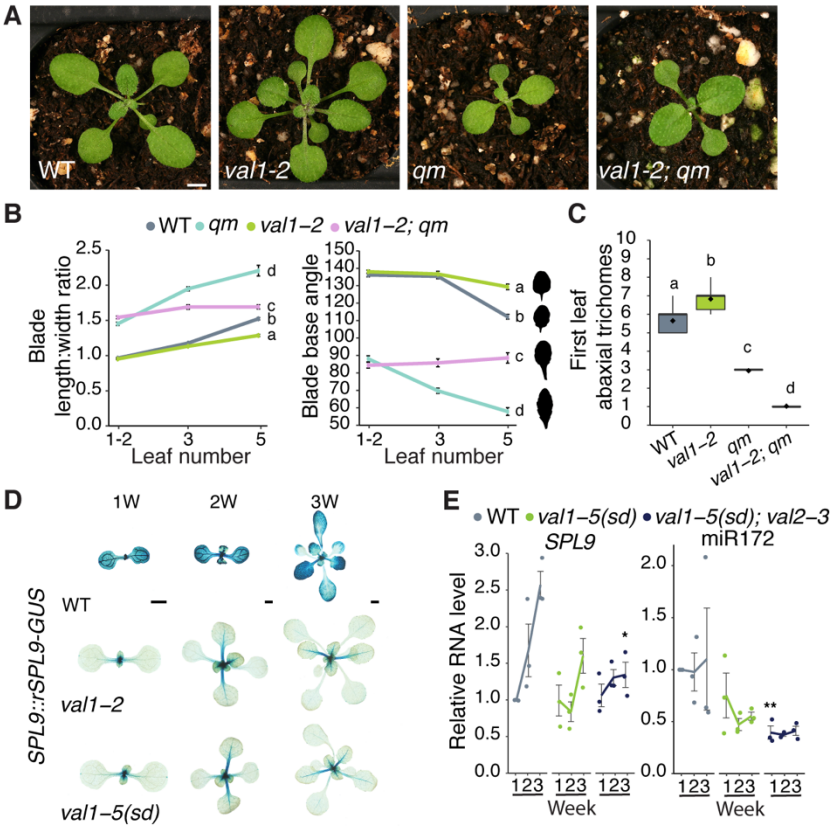

Figure 5. *VAL1* regulates vegetative phase change by miR156-dependent and independent mechanisms

(A-C) Phenotypes of *val1-2* and *mir156a mir156c mir157a mir157c quadruple mutant* lines. (A) Photographs taken at 17 DAG. Scale bar = 1mm. (B, C) Statistically distinct genotypes were identified by one-way ANOVA with *post hoc* Tukey multiple comparison test (letters indicate statistically distinct groups $P < 0.05$; (B) comparisons made at leaf 5). Bars represent the mean±s.e.m. Sample size (B) 17-60, (C) 18-36. Silhouettes in B show representative leaf 5 shapes.

(D) Expression of a miR156-resistant (*rSPL9*) reporter construct in WT, *val1-2* and *val1-5(sd)* backgrounds. Scale bars = 1mm.

(E) qRT-PCR analysis of gene expression in shoot apices with LP ≥ 1mm removed at 1, 2 and 3 weeks. Each data point represents a biological replicate and is the average of three technical replicates. Coloured lines represent the mean and gray bars represent the mean±s.e.m. Asterisk represents significant difference between WT and *val* mutant lines at the same time point, calculated by an unpaired two-tailed *t*-test with a Bonferroni correction (* $P < 0.025$; ** $P < 0.005$). All phenotypic analyses were carried out in LD conditions, the gene expression analysis was carried out in SD conditions.

424 leaves 3 and 5 (Figure 5B). This confirms that *VAL1* functions through a
425 miR156/miR157-independent mechanism to regulate vegetative phase change.
426 Surprisingly, a survey of abaxial trichome production revealed that *val1-2* enhanced this
427 aspect of the precocious *qm* phenotype (Figure 5C). This result can be explained given
428 that reduced histone deacetylation in a *toe* loss-of-function background accelerates
429 abaxial trichome formation (Wang et al., 2019), that *SPL* genes repress *TOE* activity
430 (Wu et al., 2009), and that *VAL* genes promote histone deacetylation (Zeng et al., 2020;
431 Zhou et al., 2013).

432 To determine if *VAL1* regulates *SPL* gene expression independently of miR156,
433 we crossed a miR156-resistant (*rSPL9*) *SPL9::rSPL9-GUS* reporter construct into *val1-*
434 *5(sd)*. The expression of this reporter was visibly and strongly suppressed by *val1-2* and
435 *val1-5(sd*) (Figure 5D), implying that miR156 is not required for the regulation of *SPL9*
436 by *VAL1*. The transcript levels of *SPL9*, and its target miR172, were also decreased in
437 *val* mutant plants (Figure 5E). However, it is difficult to know if this decrease is
438 dependent or independent of miR156 because miR156 induces cleavage of the *SPL9*
439 transcript (German et al., 2008; He et al., 2018; Ronemus et al., 2006).

440 VAL1/2 act as transcriptional repressors. As *SPL9* transcription decreases in *val*
441 loss-of function mutants it is therefore unlikely that VAL1/2 regulate *SPL9* directly. To
442 test this prediction, we quantified H2AK119ub and H3K27me3 at *SPL9.* Consistent with
443 previous studies, we found high levels of H2AK119ub but negligible H3K27me3 at *SPL9*
444 (Figure S5) (Li et al., 2017; Zhou et al., 2017). We also found no difference in the
445 abundance of these modifications in wild type and *val1-5(sd); val2-3* plants. Taken
446 together these results suggest that in addition to repressing *SPL9* via their effect on

447 miR156 levels, VAL1/2 repress *SPL9* indirectly through one or more miR156-
448 independent mechanisms. The observation that *val1-5(sd); val2-3* has no effect on
449 H2AK119ub at *SPL9* also suggests that *VAL1/2* are not universally required for PRC1-
450 activity.
451
452 **The effects of *VAL1* on developmental timing may be partly explained by its**
453 **expression pattern**
454 Our results show that *VAL* genes control the timing of vegetative phase change (Figure
455 1C,E), and have subtle effects on the expression pattern of miR156 during vegetative
456 development (Figure 2, S2). To determine if these effects are attributable to changes in
457 the expression level of *VAL1*, we measured the abundance of *VAL1* transcript levels
458 during vegetative growth. We observed a small but significant increase in *VAL1*
459 transcripts in shoot apices between 2 and 3 weeks of growth (Figure 6A) but there was
460 no significant change in *VAL1* levels in leaf primordia (Figure 6B). To further investigate
461 *VAL1* expression over time, we generated a *VAL1* transcriptional reporter by fusing a
462 2.3kb sequence containing the *VAL1* promoter and 5' UTR, and a 2kb sequence
463 containing the *VAL1* 3'UTR and terminator, to the GUS coding sequence (*VAL1::GUS-*
464 *VAL1 3' UTR)*. We generated a *VAL1* translational fusion by inserting a 3.8kb *VAL1*
465 genomic sequence upstream of *GUS* in this construct (*VAL1::VAL1-GUS-VAL1 3'UTR*).
466 Because the expression of the transcriptional fusion was consistently more diffuse,
467 variable, and weaker than the expression of the translational fusion (Figure S6A,B), we
468 used plants containing the translational fusion for subsequent studies.
469

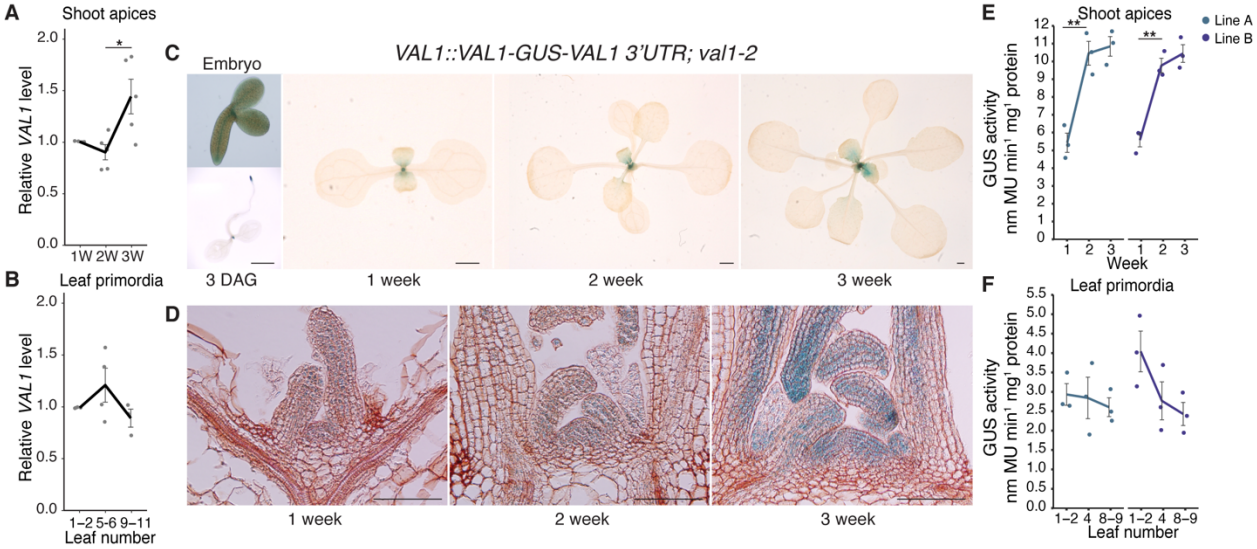

Figure 6. *VAL1* is expressed throughout vegetative development

(A, B) qRT-PCR analyses of gene expression. (A) Shoot apices with leaf primordia (LP) ≥ 1mm removed at 1, 2 and 3 weeks. (B) Isolated LP 0.5-1mm in size.

(C-F) Analyses of a *VAL1-GUS* translational fusion. (C) Expression in whole plants, scale bars = 1mm. (D) Expression in shoot apices following wax sectioning, scale bars = 0.1mm. (E, F) VAL1 levels quantified by MUG assay in two independent homozygous T3 lines. (A, B, E, F) Each data point represents a biological replicate and is the average of three technical replicates. Lines represent the mean and grey bars mean±s.e.m. Asterisks represent significant differences between two continuous time points, calculated by an unpaired two-tailed *t*-test (* $P < 0.05$; ** $P < 0.01$). All plants except the 3 DAG sample (C – long days) were grown in SD conditions.

485 During embryogenesis, the translational fusion was expressed in the root and shoot
486 apical meristems and provasculature (Figure 6C, S6A). Following germination,
487 expression became restricted to the shoot and root apices and initiating lateral root
488 primordia (Figure 6C, S6B). Throughout the rest of shoot development, the translational
489 fusion was expressed in the shoot apex and during the early stages of leaf development
490 (Figure 6C). Histological inspection indicated that *VAL1* expression increases in the
491 shoot apex during vegetative development. This was validated by a quantitative
492 analysis of GUS expression, which demonstrated that VAL1 accumulates more strongly
493 in the shoot apex than leaf primordia. Further, that VAL1 levels increase over time in the
494 shoot apex but not in older leaf primordia (Figure 6E,F). Taken together, these data
495 indicate that *VAL1* expression is restricted to apical meristems and the early stages of
496 root and leaf development. Our data also indicate that *VAL1* expression increases
497 during shoot development in very young leaf primordia, quickly declines to a uniform
498 level as the leaf develops, and ceases before the leaf is fully expanded. However, the
499 functional significance of increased VAL1 accumulation during vegetative development
500 is unclear, as we did not detect a concomitant increase in VAL1-binding to *MIR156A/C*
501 (Figure 4B, S3). Finally, the difference in the staining patterns and stability of our
502 transcriptional and translational reporters suggest that cis-regulatory elements within the
503 *VAL1* coding sequence regulate the level and site of its expression.
504 VAL1 has previously been found to physically interact with VAL2, multiple PRC1
505 and PRC2 components, and the transcriptional repressor SAP18 (Chen et al., 2018,
506 2020; Chhun et al., 2016; Jing et al., 2019; Qüesta et al., 2016; Xie et al., 2018; Yang et
507 al., 2013a; Yuan et al., 2016). However, these studies do not provide information about

508 VAL1's *in planta* protein interactions over time. To determine whether VAL1 interacts
509 with different proteins at different stages of vegetative development, we carried out a
510 mass spectrometry analysis of proteins bound to HA-tagged VAL1 at 1, 2 and 3 weeks
511 of growth. Immunoprecipitations were carried out on a *VAL1-HA; val1-2; FRI-Sf2* line,
512 using a *val1-2; fri* line as a control. The difference in the *FRI* genotype of these lines is a
513 consequence of the genotypes available at the time the experiments were performed
514 and may have had an effect on our results.

515 ATBMI1A was significantly enriched in the combined experimental samples
516 relative to the control samples (Figure 7A), which is consistent with a previous mass
517 spectrometry analysis of proteins bound to VAL1-HA (Qüesta et al., 2016). We did not
518 detect other proteins that have been identified by mass spectrometry in
519 immunoprecipitation experiments with VAL1-HA. We also observed a highly significant
520 enrichment of the chloroplast binding protein CRB. However, this is explained by the
521 enrichment of CRB in the total proteome of the experimental versus control samples
522 (Figure 7B). Comparisons of the proteins present in samples harvested from 1, 2 and 3
523 weeks old plants revealed that ATBMI1A was consistently among the most abundant
524 proteins immunoprecipitated with VAL1-HA (Figure 7C-E). The abundance of ATBMI1A
525 in the immunoprecipitated sample increased significantly from 1 week to 2 weeks, as
526 indicated by both the increase in the fold change between experimental and control
527 samples, and the statistical significance of the enrichment. This is probably a result of
528 the increase in the abundance of VAL1 between 1 and 2 weeks (Figure 6D,E), a result
529 which was confirmed by the increasing abundance of VAL1 in the immunoprecipitated
530 samples from different time points (Figure 7C-E). The parallel changes in the

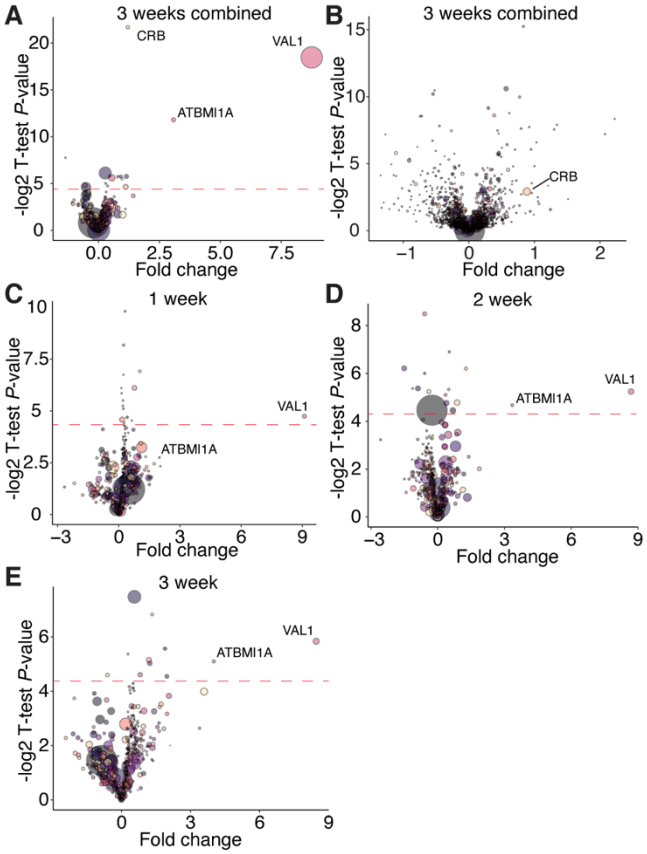

Figure 7. VAL1-protein interactions are consistent during vegetative development

(A-E) Protein enrichment calculated via mass spectrometry. Fold change represents the ratio of proteins purified from experimental (*VAL1-HA; val1-2; FRI-Sf2*) to control (*val1-2; fri*) samples, a t-test *P*-value is represented on the y-axis. Red dotted line indicates a *P*-value < 0.05 (resulting from the -log2 transformation of the actual p-value; proteins above the line have a significant enrichment). Each bubble represents an individual protein, the size or the bubble represents the protein abundance averaged across the experimental and control samples. (A, C-E) Proteins immunoprecipitated using an anti-HA antibody, (B) total proteome samples.

544 abundance of VAL1-HA and ATBMI1A, and the absence of any major change in the
545 proteins associated with VAL1-HA in different samples, suggest that the binding
546 partners of VAL1 do not change significantly during shoot development.
547 To investigate overall trends in protein accumulation during vegetative
548 development we conducted a supervised clustering analysis of the *val1-2; VAL1-HA;*
549 *FRI-Sf2* total proteome sample. We designed two clusters in which proteins either
550 increased or decreased from 1 to 2 to 3 weeks of development (see Methods for
551 details). The 50 proteins with the strongest and most consistent decreasing
552 developmental trend were significantly enriched for Gene Ontology terms related to
553 photosynthesis and carbon fixation (Figure S7 A,B). In contrast, the 50 proteins with the
554 highest increasing trend score were enriched for GO terms relating to water stress and
555 translation. The finding that younger plants invest more resources in photosynthesis is
556 consistent with a transcriptomic analysis of vegetative development in maize (Beydler et
557 al., 2016), and the enhanced photosynthetic capacity of juvenile plants at low light levels
558 (Lawrence et al., 2020).
559
560 **Discussion**
561 Plant life cycles are characterized by transitions between distinct developmental
562 phases. *VAL* genes have previously been shown to promote the switch from
563 embryogenesis to seed maturation (Suzuki et al., 2007; Yang et al., 2013a), and from
564 vegetative to reproductive growth (Qüesta et al., 2016; Yuan et al., 2016). The results
565 presented here demonstrate that *VAL1* and *VAL2* also regulate the intervening

566 transition from juvenile to adult stages of vegetative growth. *VAL* genes thus function as
567 a regulatory hub that coordinates developmental transitions throughout plant life cycles.
568
569 Regulation of miR156 expression by *VAL1/2*
570 Vegetative phase change is promoted by a temporal decline in miR156/miR157
571 expression (Wu and Poethig, 2006). When the level of miR156/miR157 falls below a
572 specific threshold, the de-repression of *SPL* genes initiates a switch to adult identity.
573 Previous work has shown that – with the exception of *SPL3* – the increase in *SPL*
574 transcript levels during development is entirely attributable to post-transcriptional
575 regulation by miR156/miR157 (He et al., 2018). Factors that control the timing of
576 vegetative phase change can therefore act in three ways: 1) by modifying the rate of
577 decline in miR156; 2) by constitutively increasing or decreasing the level of miR156; and
578 3) by constitutively increasing or decreasing the rate of transcription of *SPL* genes. Our
579 results suggest that *VAL1* and *VAL2* regulate vegetative phase change both by
580 constitutively decreasing the level of miR156 and by repressing *SPL* gene expression
581 independently of miR156.
582 Evidence that *VAL1/VAL2* constitutively regulate the level of miR156 was
583 provided by the phenotype of plants deficient for *VAL1* and *VAL2*, VAL1-DNA binding
584 patterns and from the phenotype of plants expressing a *MIR156C* transgene lacking
585 VAL-binding sites. We found that although *VAL1* expression increases in the shoot apex
586 as plants develop, *val1; val2* double mutants displayed only a slight decrease in the rate
587 at which miR156 declines. Instead, *val1; val2* double mutants exhibited a significant
588 increase in the level of miR156 at every stage of vegetative development we examined.

589 Consistent with this result, *mir156a; mir157a; mir157c* triple mutants transformed with a
590 *MIR156C* transgene lacking VAL-binding sites had elevated levels of miR156 relative to
591 the wild type *MIR156C* control, but displayed the same temporal decrease in miR156 as
592 control plants.

593 We have proposed that the decrease in *MIR156A/C* expression during shoot
594 development may be attributable to the stochastic replacement of H3K27ac and
595 H3K4me3 by H3K27me3 (Xu et al., 2018, 2016b). The observation that the increase in
596 miR156 expression in *val1; val2* is associated with a decrease in the level of H3K27me3
597 at *MIR156C* supports this hypothesis, in that it shows that H3K27me3 is associated with
598 low levels of *MIR156C* expression. The difference in the phenotype of plants doubly
599 mutant for *val1-2* and mutations the PRC2 histone methyltransferases, *SWN* and *CLF*,
600 and between *val1-2* and a mutation in the histone deacetylase *HDA19*, supports the
601 hypothesis that the expression of *MIR156C* is regulated by a combination of histone
602 marks. *val1-2; swn-3* and *val1-2; clf-29* double mutants have approximately the same
603 amount of miR156 as *val1-2* single mutants, which is expected given that these genes
604 are involved in the same process, namely the deposition of H3K27me3. In contrast,
605 *hda19-3* significantly enhanced the level of miR156 compared to *val1-2*. This type of
606 genetic interaction is predicted if miR156 expression is dependent on histone
607 modifications aside from H3K27me3.

608 The evidence that *VAL1/VAL2* regulate the level, but not the temporal expression
609 pattern, of miR156 leaves open the question of how its temporal pattern arises. Several
610 other chromatin regulators, such as the CHD3 nucleosome remodeler PICKLE (Xu et
611 al., 2016b), the PRC-accessory protein LHP1 (Cui et al., 2020), the SWI/SNF2

612 chromatin remodeler BRAHMA (Xu et al., 2016c), and the histone 2 regulators ARP6
613 and HTA9/11 (Choi et al., 2016; Xu et al., 2018) have been found to play a role in the
614 expression of miR156. Furthermore, transcription factors including AGL15/18
615 (Serivichyaswat et al., 2015), MYB33 (Guo et al., 2017), and members of the *NF-Y*
616 family (Wei et al., 2017; Zhao et al., 2020), also regulate miR156 expression. It is
617 possible that the temporal expression pattern of miR156 is a consequence of complex
618 interactions between these diverse factors, rather than being dependent on a single
619 class of regulator, such as *VAL1/2*.
620
621 *VAL* genes and PRC1 activity
622 *VAL1/2* are thought to be necessary for the recruitment of PRC1 to target loci,
623 where it represses gene expression via PRC2-dependent and independent mechanisms
624 (Baile et al., 2020; Yuan et al., 2020; Zhou et al., 2017). We found that *VAL1/2*
625 accelerate vegetative phase change by repressing the expression of *MIR156A/C*, and
626 by indirectly promoting the expression of *SPL9*, a target of miR156. These results are
627 consistent with a previous study (Pico et al., 2015), which showed that *VAL1/2* and the
628 PRC1 components, AtBMI1A/B, repress *MIR156A/C* expression. However, the PRC1
629 components EMBRYONIC FLOWER1 (Pico et al., 2015) and RING1A/B (Li et al., 2017)
630 have also been reported to repress the expression of *SPL9* independently of miR156.
631 These latter effects delay vegetative phase change, which is the exact opposite of the
632 effect produced by PRC1-mediated repression of *MIR156A/C*. Together, these results
633 indicate that PRC1 can operate at different points within a regulatory pathway, or in
634 interacting regulatory pathways, to modulate the output of the pathway or pathways. If

635 the genes repressed by PRC1 have different functions—as in the case of miR156 and
636 its *SPL* targets—then the functional significance of a particular level of PRC1 activity at
637 a particular locus can be difficult to predict. These results also support the hypothesis
638 that there may be different forms of PRC1, which target different genes. Moreover, our
639 finding that H2AK119ub deposition at *SPL9* was unaffected in *val1-5(sd); val2-3*
640 suggests that VAL1/2 may not be universally required for PRC1-recruitment.

641 In this regard, it is interesting that although *MIR156A* and *MIR156C* are close
642 paralogs and have similar expression patterns, previous studies (Xu et al., 2018,
643 2016b), and the results presented here, indicate that these genes are differentially
644 sensitive to mutations that affect the activity of PRC2 and PRC1. For example, we found
645 that *val1; val2* mutants display a greater reduction in H2AK119ub and H3K27me3 at
646 *MIR156C* than at *MIR156A*. Our findings align with the results of ChIP-seq studies of
647 H2AK119ub and H3K27me3 in *atbmi1a/b/c* (Zhou et al., 2017) and *val1-2; val2-3* (Yuan
648 et al., 2020) mutants. The implication of these observations is that *MIR156C* expression
649 is more dependent on PRC1 and PRC2 activity than *MIR156A.* Defining the molecular
650 basis for this difference could provide important insights into factors that influence
651 epigenetic regulation in plants.

652 Unlike in animals, where PRC1 binding requires the prior deposition of
653 H3K27me3, in plants PRC1 is thought to promote PRC2 activity at the majority of its
654 targets (Calonje, 2014; Zhou et al., 2017). This model is supported by our results. In the
655 case of *MIR156C*, we found that in 1 week old plants loss of *VAL1/2* significantly
656 reduced H2AK119ub, but not H3K27me3. However, by 3 weeks both H2AK119ub and
657 H3K27me3 were reduced in *val1/2* mutants. These results suggest that VAL1/2 and, by

658 inference, PRC1 are present at *MIR156C* prior to PRC2, and promote the activity of
659 PRC2.

660 In addition to their roles in vegetative phase change, *VAL* genes regulate multiple
661 nodes of the flowering time (Jing et al., 2019; Qüesta et al., 2016; Yuan et al., 2016)
662 and seed development (Chen et al., 2018, 2020; Suzuki et al., 2007; Yang et al., 2013a)
663 networks. The co-option of *VAL* activity throughout genetic networks thus appears
664 critical to coordinating plant developmental transitions. Despite the centrality of *VAL*
665 function to the control of developmental timing, the persistent and robust pattern of
666 *MIR156A/C* expression in *val* mutant plants emphasizes the complexity of temporal
667 regulation in plants.

668

669 **Acknowledgements**

670 We thank members of the R.S.P laboratory and Doris Wagner (University of
671 Pennsylvania) for helpful discussions, Daniel Martinez and Ryan McCarthy (University
672 of Pennsylvania) for assistance with histology and chromatin sonication, the Arabidopsis
673 Biological Resource Center for T-DNA insertion lines and Julia Qüesta and Caroline
674 Dean (John Innes Center) for the kind donation of *VAL1-HA; val1-2; FRI-Sf2* seed. This
675 project was funded by NIH Grant GM051893 (to R.S.P). S.S. gratefully acknowledges
676 Merck/MSD for the Umberto Mortari Award (2019), the Japan Agency for Medical
677 Research and Development (AMED) and the New York Academy of Sciences (NYAS)
678 for supporting his lab in aging research.

679

680 **Author Contributions**

681 Conceptualization: J.P.F., R.S.P.; Methodology: J.P.F., R.S.P.; Investigation: J.P.F.,
682 J.H., V.J.C., S.S.; Formal analysis: J.P.F., S.S.; Resources: J.P.F., J.H.; Visualization:
683 J.P.F., S.S.; Writing - original draft: J.P.F.; Writing - review & editing: J.P.F., J.H., S.S.,
684 R.S.P.; Supervision: R.S.P.; Project administration: R.S.P.; Funding acquisition: R.S.P.
685
686 **Declaration of Interests**
687 The authors declare no competing interests.
688
689 **Figure titles and legends**
690 **Figure 1. *VAL* genes redundantly regulate vegetative phase change**
691 (C) Schematic of *val1* and *val2* alleles used in this study – grey boxes represent
692 UTRs, black boxes represent exons, red triangles represent T-DNA insertions,
693 red line represents EMS-induced base substitution.
694 (D) Phenotypes at 21 DAG in LD conditions, scale bar = 5mm.
695 (C-E) Quantitative analysis of vegetative development. Statistically distinct genotypes
696 were identified by one-way ANOVA with *post hoc* Tukey multiple comparison test
697 (letters indicate statistically distinct groups $P < 0.05$; for (E) comparisons were
698 made at leaf 5), all plants grown in LD. (C,D) Boxes display the interquartile
699 range (IQR) (boxes), median (lines) and values beyond 1.5*IQR (whiskers);
700 mean values are marked by ◆. (E) Colored lines represent the mean and black
701 bars the SEM. Sample sizes (C, D) 21-46, (E) 13-46.
702

703 **Figure 2. *VAL* genes function predominantly as quantitative regulators of miR156**
704 **expression**

705 (A, B) qRT-PCR analyses of gene expression. (A) Shoot apices with leaf primordia (LP)
706 ≥ 1mm removed at 1, 2 and 3 weeks. (B) Isolated LP 0.5-1mm in size. All plants
707 were grown in SD conditions. Each data point represents a biological replicate
708 and is the average of three technical replicates. Coloured lines represent the
709 mean and black bars mean±s.e.m. Asterisks represent significant differences
710 between WT and *val* mutants at the same time point, calculated by an unpaired
711 two-tailed *t*-test with a Bonferroni correction for multiple comparisons (* $P <$
712 0.025; ** $P < 0.005$; *** $P < 0.0005$).

713

714 **Figure 3. *VAL* genes regulate miR156 activity via-PRC2 and PRC1**

715 (B) Schematics of the primer locations used for ChIP-qPCR. Blue and green bars
716 represent sequences encoding the mature miRNA and miRNA hairpin
717 respectively.

718 (B) Temporal analysis of H3K27me3 by ChIP-qPCR. Each data point represents a
719 biological replicate and is the average of three technical replicates. Lines
720 represent the mean, bars represent the mean±s.e.m., asterisks represent
721 significant differences between WT and *val1-5(sd); val2-3* at the same time point,
722 calculated by an unpaired two-tailed *t*-test (* $P < 0.05$; ** $P < 0.01$; *** $P < 0.001$).
723 H3K2me3 values are relative to H3 and normalised to *STM* as an internal control.
724 Plants were grown in SD conditions.

725 (C, D) Phenotypes in LD. (D) Photographs taken at 21DAG, scale bar = 5mm. (E)
726 Asterisks represent significant differences to either WT or *val1-2*, calculated by
727 unpaired two-tailed *t*-test with Bonferroni correction for multiple comparisons (***
728 $P < 0.00033$). Sample size 22-46.
729 (G) qRT-PCR analyses of gene expression in shoot apices with LP ≥ 1mm removed
730 at 1, 2 and 3 weeks. Each data point represents a biological replicated and is the
731 average of three technical replicates. Coloured lines represent the mean and
732 black bars represent the mean±s.e.m. Asterisks represent significant differences
733 between *val1-2* and *val1-2; clf-29/val1-2; swn-3/val1-2; hda19-3* at the same time
734 point, calculated by unpaired two-tailed *t*-test with Bonferroni correction for
735 multiple comparisons (** $P < 0.0033$). Plants were grown in SD conditions.
736 (H) Temporal analysis of H2AK119ub by ChIP-qPCR, values are relative to input and
737 normalised to *ACT7* as an internal control. See (B) for details.
738
739 **Figure 4. Loss of RY VAL-binding motifs at the *MIR156C* locus delays vegetative**
740 **phase change**
741 (C) Schematic depicting the location of primers used for ChIP-qPCR, the sequences
742 encoding the miR156 hairpin and mature miRNA are coloured green and blue
743 respectively.
744 **(D)** Anti-HA ChIP-qPCR of WT Col control plants at 2W and *VAL1::VAL1-HA; val1-2;*
745 *FRI-Sf2* plants at 1, 2 and 3W of growth. The data is presented as percentage
746 input normalized to *ACT7* and is displayed relative to WT. Each data point

747 represents a biological replicate and is the average of three technical replicates,
748 bars represent the mean and error bars the mean±s.e.m.
749 (C, D) Phenotypes of T1 plants transformed with *MIR156C* RY variants. Statistically
750 distinct genotypes were identified by one-way ANOVA with *post hoc* Tukey
751 multiple comparison test (letters indicate statistically distinct groups $P < 0.05$;
752 comparison in (C) made at leaf 5). *qm = mir156a mir156c mir157a mir157c*
753 *quadruple mutant, tm = mir156a mir157a mir157c triple mutant,* EV = empty
754 vector. (C) Colored lines represent the mean and black bars the mean±s.e.m.
755 Sample size (B) 26-52, (C) 37-51.
756 (E) qRT-PCR analyses of gene expression in shoot apices with LP ≥ 1mm removed
757 at 1, 2 and 3 weeks. Each data point represents an independent homozygous T3
758 line and is the average of three technical replicates. Colored lines represent the
759 mean and black bars the mean±s.e.m. Asterisks represent significant differences
760 between *qm; MIR156C* and *qm; MIR156C -RY* lines at the same time point,
761 calculated by an unpaired two-tailed *t*-test with a Bonferroni correction for
762 multiple comparisons (* $P < 0.025$, ** $P < 0.005$).
763 (G) Genetic interaction between *val1-2* and *MIR156C* RY deletions. Asterisks
764 represent significant differences between plants with wild type or null *VAL1*
765 alleles calculated by an unpaired two-tailed *t*-test (*** $P < 0.001$). Sample size
766 24-36. Phenotyping analyses were carried out in LD conditions, gene expression
767 and ChIP analyses were carried out in SD conditions.
768

769 **Figure 5. *VAL1* regulates vegetative phase change by miR156-dependent and**
770 **independent mechanisms**

771 (A-C) Phenotypes of *val1-2* and *mir156a mir156c mir157a mir157c quadruple mutant*
772 lines. (A) Photographs taken at 17 DAG. Scale bar = 1mm. (B, C) Statistically
773 distinct genotypes were identified by one-way ANOVA with *post hoc* Tukey
774 multiple comparison test (letters indicate statistically distinct groups $P < 0.05$; (B)
775 comparisons made at leaf 5). Bars represent the mean±s.e.m. Sample size (B)
776 17-60, (C) 18-36. Silhouettes in B show representative leaf 5 shapes.

777 (F) Expression of a miR156-resistant (*rSPL9*) reporter construct in WT, *val1-2* and
778 *val1-5(sd)* backgrounds. Scale bars = 1mm.

779 (G) qRT-PCR analysis of gene expression in shoot apices with LP ≥ 1mm removed
780 at 1, 2 and 3 weeks. Each data point represents a biological replicate and is the
781 average of three technical replicates. Coloured lines represent the mean and
782 gray bars represent the mean±s.e.m. Asterisk represents significant difference
783 between WT and *val* mutant lines at the same time point, calculated by an
784 unpaired two-tailed *t*-test with a Bonferroni correction (* $P < 0.025$; ** $P < 0.005$).
785 All phenotypic analyses were carried out in LD conditions, the gene expression
786 analysis was carried out in SD conditions.

787

788 **Figure 6. *VAL1* is expressed throughout vegetative development**

789 (A, B) qRT-PCR analyses of gene expression. (A) Shoot apices with leaf primordia (LP)
790 ≥ 1mm removed at 1, 2 and 3 weeks. (B) Isolated LP 0.5-1mm in size.

791 (C-F) Analyses of a *VAL1-GUS* translational fusion. (C) Expression in whole plants,
792 scale bars = 1mm. (D) Expression in shoot apices following wax sectioning, scale
793 bars = 0.1mm. (E, F) VAL1 levels quantified by MUG assay in two independent
794 homozygous T3 lines. (A, B, E, F) Each data point represents a biological
795 replicate and is the average of three technical replicates. Lines represent the
796 mean and grey bars mean±s.e.m. Asterisks represent significant differences
797 between two continuous time points, calculated by an unpaired two-tailed *t*-test (*
798 $P < 0.05$; ** $P < 0.01$). All plants except the 3 DAG sample (C – long days) were
799 grown in SD conditions.
800
801 **Figure 7. VAL1-protein interactions are consistent during vegetative development**
802 (A-E) Protein enrichment calculated via mass spectrometry. Fold change represents
803 the ratio of proteins purified from experimental (*VAL1-HA; val1-2; FRI-Sf2*) to
804 control (*val1-2; fri*) samples, a t-test *P*-value is represented on the y-axis. Red
805 dotted line indicates a *P*-value < 0.05 (resulting from the -log2 transformation of
806 the actual p-value; proteins above the line have a significant enrichment). Each
807 bubble represents an individual protein, the size or the bubble represents the
808 protein abundance averaged across the experimental and control samples. (A,
809 C-E) Proteins immunoprecipitated using an anti-HA antibody, (B) total proteome
810 samples.
811
812 **STAR methods**
813 **KEY RESOURCES TABLE**

RESOURCE AVAILABILITY

Lead Contact

Further information and requests for resources and reagents should be directed to, and will be fulfilled by, the Lead Contact Scott Poethig (spoethig@sas.upenn.edu).

Materials Availability

The *val1-5(sd), val1-5(sd); val2-3*, *val1-2; val2-4, val1-2; mir156ac mir157ac* and *VAL1::VAL1-GUS-VAL1 3'UTR* lines described herein have been donated to the ABRC (stock numbers CS72451-CS72455 respectively). All other plant lines and plasmids generated during this project are available on request to Scott Poethig (spoethig@sas.upenn.edu).

Data and Code Availability

The raw files from the experiments performed with mass spectrometry are deposited on the free repository Chorus (https://chorusproject.org) at Project No. 1706.

EXPERIMENTAL MODELS AND SUBJECT DETAILS

Plant material and growth conditions

All stocks were grown in the Col-0 background. The following genetic lines have been described previously: *val1-2* (SALK_088606)*, val2-1* (CS906036) (Suzuki et al., 2007) (*val2-1* was backcrossed to Col-0 6 times from the original Wassilewskija parent); *val2-3* (SALK_059568C) (Yang et al., 2013a); *clf-29* (SALK_021003) (Bouveret et al., 2006);

837 *swn-3* (SALK_050195) (Chanvivattana et al., 2004); *hda19-3* (SALK_139445) (Kim et
838 al., 2008); *mir156a-2 mir156c-1 mir157a-1 mir157c-1* (He et al., 2018); *SPL9::rSPL9-*
839 *GUS* (Xu et al., 2016a); *val1-2 VAL1::VAL1-3xHA FRI-Sf2* (Qüesta et al., 2016). *val2-4*
840 (SALK_127961) was obtained from the Arabidopsis Biological Resources Center (Ohio
841 State University, OH, USA). Seeds were sown on fertilized Farfard #2 soil (Farfard) and
842 kept at 4°C for 3 days prior to transfer to a growth chamber, with the transfer day
843 counted as day 0 for plant age (0 DAG – days after germination). Plant were grown at
844 22°C under a mix of both white (USHIO F32T8/741) and red-enriched (Interlectric
845 F32/T8/WS Gro-Lite) fluorescent bulbs in either long day (16 hrs light/8 hrs. dark; 40
846 μmol m^{-2} s^{-1}) or short day (10 hrs light/14 hrs dark; 100 μmol m^{-2} s^{-1}) conditions.
847

848 **Identification of the *val1-5(sd)* mutant**

849 The *val1-5(sd)* allele was generated by exposing *mir157a-1; mir157c-1* seed to ethyl
850 methanesulfonate. An M2 mutant plant exhibiting delayed vegetative phase change was
851 backcrossed to the parental line and allowed to self. Tissue was pooled from 30 plants
852 exhibiting severely delayed vegetative phase change in the BC1F2 generation. DNA
853 was extracted via-SDS lysis and phenol-chloroform extraction and further purified using
854 Clean and Concentrator columns (Zymo Research). DNA concentration was determined
855 using a Qubit 2.0 Fluorometer (Invitrogen) and 1μg of DNA sheared using a Covaris S2
856 sonicator (Covaris) to produce 350bp inserts. Sequencing libraries were made following
857 the TruSeq DNA PCR-free LT Sample Prep Kit (Illumina) manufacturer's instructions.
858 Library quality and quantity was validated by Bioanalyser (Agilent) and KAPA analysis
859 (Kapa Biosystems). 100bp paired end reads were generated using a HiSeq 2500

860 (Illumina) and aligned to the TAIR10 reference genome following the default SHORE
861 pipeline (Ossowski et al., 2008). The SHOREmap backcross pipeline (Schneeberger et
862 al., 2009) using default options was employed to identify polymorphisms. Manual
863 inspection of allele frequencies in the mutant revealed a peak centered on the *VAL1*
864 locus. The causative mutation was confirmed by Sanger sequencing and
865 complementation assays. The mutant was backcrossed to a 'Traffic Line' (Wu et al.,
866 2015) with seed-fluorescent markers inserted adjacent to the *VAL1* locus to eliminate
867 additional closely linked polymorphisms. Consequently, the resultant *val1-5(sd)* plants
868 used in this study contain a linked *pNAP::RFP* insertion at 13,622,737bp on
869 Chromosome 2 (Crick strand).
870
871 **Generation of transgenic plants**
872 For RY-mutation lines the RY-site TGCATG was replaced by TGTATG. A 5kb *MIR156C*
873 genomic sequence including 2kb upstream of the transcriptional start site and 665bp
874 downstream of the end of the last exon was cloned into the binary vector pAGM4723
875 from the Golden Gate MoClo toolbox supplied by Addgene (www.addgene.org) (Weber
876 et al., 2011; Werner et al., 2012). For -RY3, -RY4 and -RY5 Q5 Site Directed
877 Mutagenesis Kit (New England Biolabs) was used to induce a substitution directly into
878 the expression vector. For -RY1, -RY2 and -RY12345 Gibson Assembly cloning (New
879 England Biolabs) was used to assemble individual fragments into the same backbone.
880 Golden Gate cloning was also used to generate *VAL1::VAL1-VAL1 3'UTR*,
881 *VAL1::VAL1-GUS-VAL1 3'UTR*, *VAL1::GUS-VAL1 3'UTR* lines. Promoter/5'UTR (*VAL1*

882 - 2.3kb), functional (*VAL1* – 3.8kb, *MIR156A* (Fouracre and Poethig, 2019)) and
883 3'UTR/terminator (*VAL1* – 2kb) sequences were cloned separately from *Arabidopsis*
884 gDNA, with Type II restriction sites removed where necessary. *GUS* and *AtuOCS*
885 sequences were obtained from the MoClo Plant Parts toolkit supplied by Addgene
886 (www.addgene.org) (Engler et al., 2014). Component parts were assembled using
887 Golden Gate cloning into the pAGM4723 binary vector, including green or red seed
888 fluorescent expression cassettes as selectable markers. Constructs were transformed
889 into *Arabidopsis* using the floral dip method. All primers used for cloning are included in
890 Table S1.
891
892 **METHOD DETAILS**
893 **Quantification of gene expression**
894 Tissue (either shoot apices with leaf primordia ≤1mm attached or isolated leaf primordia
895 0.5-1mm in size – as specified in the text) were ground in liquid nitrogen and total RNA
896 extracted using Trizol (Invitrogen) as per the manufacturer's instructions. RNA was
897 treated with RNAse-free DNAse (Qiagen) and 250ng-1µg of RNA was used for reverse
898 transcription using Superscript III (Invitrogen). Gene specific RT primers were used to
899 amplify miR156, miR157, miR172 and SnoR101 and a polyT primer for mRNA
900 amplification. Three-step qPCR of cDNA was carried out using SYBR-Green Master Mix
901 (Bimake). qPCR reactions were run in triplicate and an average was calculated.
902 Relative transcript levels were normalized to snoR101 (for miRNAs) and *ACT2* (for
903 mRNAs) and expressed as a ratio of expression to a specified control sample. The
904 qPCR primers used in this study are listed in Table S1.

905

906 **Chromatin immunoprecipitation**

907 Expanded leaves and roots were removed during tissue harvesting to produce samples
908 enriched for shoot apices and young leaves. For histone ChIP ~0.5g of fresh tissue per
909 antibody and for anti-HA ChIP ~5g of fresh tissue were harvested. Samples were fixed
910 in 1% formaldehyde under vacuum for 15 minutes. Cross-linked samples were ground
911 in liquid nitrogen and suspended in Honda buffer (0.44M sucrose, 1.25% ficoll, 2.5%
912 dextran 40, 20mM hepes pH 7.4, 10mM $MgCl_2$, 0.5% Triton, 5mM DTT, 1mM PMSF,
913 1% protease inhibitors), filtered through two layers of Miracloth (EMD Millipore), and
914 pelleted and washed thrice in Honda buffer. For histone ChIP, pellets were
915 resuspended in nuclei lysis buffer (50mM Tris-HCl pH 8, 10mM EDTA, 1% SDS, 1%
916 protease inhibitors), for anti-HA ChIP, pellets were resuspended in RIPA buffer (1X
917 PBS, 1% NP-40, 0.5% sodium deoxycholate, 0.1% SDS, 1% protease inhibitors).
918 Samples were sonicated using a Fisherbrand Sonic Dismembrator (Fisher Scientific) 6x
919 10s at setting 3.2. ChIP samples were pre-cleared using Dynabeads Protein A
920 (Invitrogen). 2% was removed as input and samples were incubated overnight with 1%
921 antibody (for histone ChIP: anti-H3 (abcam ab1791), anti-H3K27me3 (EMD Millipore 07-
922 449), anti-H2AK119ub (Cell Signaling Technology 8240); for VAL1-HA ChIP: anti-HA
923 (Roche 11583816001)). Chromatin-antibody conjugates were purified with Dynabeads
924 Protein A and washed in low/high salt, lithium and TE buffers. Following reverse-
925 crosslinking DNA was isolated using a QIAquick PCR Purification Kit (Qiagen).

926 For ChIP-qPCR assays, three-step qPCR was carried out using SYBR-Green
927 Master Mix (Bimake). qPCR reactions were run in triplicate and an average was

928 calculated. Data were normalized and presented as follows: 1) For H3K27me3 – *STM*
929 was used as a control locus, data is presented as a ratio of (H3K27me3 gene of
930 interest/H3 gene of interest) to (H3K27me3 *STM*/H3 *STM*); 2) For H2AK119ub – *ACT7*
931 was used as a control locus, data is presented as a ratio of (H2AK119ub gene of
932 interest/input gene of interest) to (H2AK119ub *ACT7*/input *ACT7*); 3) For VAL1-HA –
933 *UBQ10, ACT7* and *TA3* were used as control loci, data is presented as a ratio of
934 ((VAL1-HA ChIP gene of interest/input gene of interest)/(VAL1-HA ChIP control/input
935 control)) relative to ((WT ChIP gene of interest/input gene of interest)/(WT ChIP
936 control/input control)). The qPCR primers used in this study are listed in Table S1.
937
938 **Mass spectrometry**
939 *VAL1::VAL1-3xHA; val1-2; FRI-Sf2* and *val1-2* genotypes were used as experimental
940 and control samples respectively. Expanded leaves and roots were removed during
941 tissue harvesting to produce samples enriched for shoot apices and young leaves. 2-3g
942 of fresh tissue was harvested for immunoprecipitation, 0.2-0.6g was harvested for total
943 protein extraction. For immunoprecipitation, tissue was ground in liquid nitrogen,
944 suspended in IP buffer (20mM Tris-HCl pH 8, 150mM NaCl, 2.5mM EDTA, 0.5% Triton,
945 1% protease inhibitors, 1mM PMSF), rotated for 2 hours at 4°C and filtered through 2
946 layers of Miracloth. Anti-HA (Roche) conjugated Dynabeads Protein A (Invitrogen) were
947 added and samples were rotated overnight at 4°C. Beads were washed thrice with IP
948 buffer and proteins were purified for mass spectrometry using an S-Trap: Rapid
949 Universal MS Sample Prep (Protifi) following the manufacturer's instructions. For total
950 proteomes, ground tissue was suspended in 8M urea and rotated at room temperature

951 for 45 minutes. The samples were centrifuged thrice and the supernatant reduced with
952 DTT (final concentration 5mM) and alkylated with iodoacetamide 40 (final concentration
953 40mM) before overnight digest with trypsin. Samples were resuspended in 10 µl of
954 water + 0.1% TFA and loaded onto a Dionex RSLC Ultimate 300 (Thermo Scientific,
955 San Jose, CA, USA), coupled online with an Orbitrap Fusion Lumos (Thermo Scientific).
956 Chromatographic separation was performed with a two-column system, consisting of a
957 C_{18} trap cartridge (300 µm ID, 5 mm length) and a picofrit analytical column (75 µm ID,
958 25 cm length) packed in-house with reversed-phase Repro-Sil Pur C_{18}-AQ 3 µm resin.
959 Peptides were separated using a 90 min gradient (for the IP experiments) and 180 min
960 (for the full proteome experiment) from 2-28% buffer-B (buffer-A: 0.1% formic acid,
961 buffer-B: 80% acetonitrile + 0.1% formic acid) at a flow rate of 300 nl/min. The mass
962 spectrometer was set to acquire spectra in a data-dependent acquisition (DDA) mode.
963 Briefly, the full MS scan was set to 300-1200 m/z in the orbitrap with a resolution of
964 120,000 (at 200 m/z) and an AGC target of 5x10e5. MS/MS was performed in the ion
965 trap using the top speed mode (2 secs), an AGC target of 10e4 and an HCD collision
966 energy of 30. Raw files were searched using Proteome Discoverer software (v2.4,
967 Thermo Scientific) using SEQUEST as search engine using the SwissProt *Arabidopsis*
968 *thaliana* database. The search for total proteome included variable modifications of
969 methionine oxidation and N-terminal acetylation, and fixed modification of
970 carbamidomethyl cysteine. Trypsin was specified as the digestive enzyme. Mass
971 tolerance was set to 10 pm for precursor ions and 0.2 Da for product ions. Peptide and
972 protein false discovery rate was set to 1%. Data transformation, normalization and

973 statistical analysis using heteroscedastic t-test was performed as previously described
974 (Aguilan et al., 2020).
975 Proteins were sorted according to their descending or ascending linearity across
976 the three weeks. To do so, we used a custom score taking into account monotonic
977 trend, reproducibility across replicates and magnitude of change across weeks. The 50
978 proteins with the highest descending and ascending trend scores were used to identify
979 enriched GO terms for biological processes using the Fisher's Exact PANTHER
980 Overrepresentation Test (released 2020-07-28) and GO Ontology database DOI:
981 10.5281/zenodo.4081749 (released 2020-10-09). The *Arabidopsis thaliana* genome
982 was used as a reference list. Protein interaction maps for the same sets of 50 proteins
983 were made using the STRING app from Cytoscape (Shannon et al., 2003).
984
985
986 **GUS staining and histology**
987 Shoot apices and whole plants were fixed in 90% acetone on ice for 10 minutes,
988 washed with GUS staining buffer (5mM potassium ferricyanide and 5mM ferrocyanide in
989 0.1M PO_4 buffer) and incubated at 37°C overnight in GUS staining buffer with 2mM X-
990 Gluc. Embryos were placed directly in X-Gluc (GoldBio) GUS staining buffer and
991 incubated for 1hr. To quantify GUS activity, a 4-methylumbelliferyl b-D-glucuronide
992 (MUG) (Sigma-Aldrich) assay was carried out as previously described (He et al., 2018).
993 For histological observations individuals were fixed in FAA (3.7% formaldehyde),
994 dehydrated in an ethanol series and cleared using Histo-Clear (National Diagnostics).
995 Following embedding in Paraplast Plus (Sigma-Aldrich) 8μM sections were produced

996 using an HM 355 microtome (Microm) and visualized using an Olympus BX51
997 microscope with a DP71 camera attachment (Olympus).
998
999 **QUANTIFICATION AND STATISTICAL ANALYSES**
1000 Details of all statistical analyses, including the type of statistical test, sample size,
1001 replicate number and significance threshold, are included in the relevant figure legend.
1002 For figures featuring boxplots, boxes display the IQR (boxes), median (lines), and
1003 values beyond 1.5* IQR (whiskers); mean values are marked by a solid diamond (◆).
1004 Statistical analyses were carried out using RStudio (RStudio Team, 2020) and Microsoft
1005 Excel. Measurements of leaf shape were made using ImageJ (Schindelin et al., 2012).
1006
1007 **Supplemental Information titles and legends**
1008 **Figure S1. *val1-5(sd)* is an antimorphic allele**
1009 (A) Sequence alignment of the B3 DNA-binding domain N-arm of *Arabidopsis* LAV
1010 family members and the maize ABI3 ortholog VP1. Numbers correspond to
1011 amino acid sequence numbers, colors correspond to the ClustalX amino acid
1012 color scheme. In the *val1-5(sd)* mutant a C>T base substitution converts an
1013 arginine to a cysteine.
1014 (B) *val1-5(sd)* complementation test with the null *val1-2* allele
1015 (C) Rescue of the *val1-5(sd)* abaxial trichome phenotype with a *VAL1* genomic
1016 sequence. Independent T1 lines are shown.
1017 (D) Allele heterozygosity testing. (B-D) Boxes display the interquartile range (IQR)
1018 (boxes), median (lines) and values beyond 1.5*IQR (whiskers); mean values are

1019 marked by ◆. Samples sizes are displayed on the graph. Statistically distinct
1020 genotypes were identified by one-way ANOVA with *post hoc* Tukey multiple
1021 comparison test (letters indicate statistically distinct groups; $P < 0.05$), all plants
1022 grown in LD.
1023 (E) Heteroblastic series of lines shown in Figure 1.
1024
1025 **Figure S2. *VAL* genes redundantly regulate miR156 expression**
1026 qRT-PCR analyses of gene expression in shoot apices with leaf primordia (LP) ≥
1027 1mm removed at 1, 2 and 3 weeks. All plants were grown in SD conditions. Each
1028 data point represents a biological replicate and is the average of three technical
1029 replicates. Coloured lines represent the mean and black lines mean±s.e.m.
1030 Asterisks represent significant differences between WT and *val* mutants at the
1031 same time point, calculated by an unpaired two-tailed *t*-test with a Bonferroni
1032 correction for multiple comparisons (* $P < 0.025$; ** $P < 0.005$; *** $P < 0.0005$).
1033
1034 **Figure S3. VAL1 binds consistently to *MIR156A* and *MIR156C* during vegetative**
1035 **development**
1036 (A) Schematic depicting the location of primers used for ChIP-qPCR, the sequences
1037 encoding the miR156 hairpin and mature miRNA are coloured green and blue
1038 respectively.
1039 (B) Anti-HA ChIP-qPCR of WT Col control plants at 2W and *VAL1::VAL1-HA; val1-2;*
1040 *FRI-Sf2* plants at 1, 2 and 3W of growth. The data is presented as percentage
1041 input normalized to a control locus (*UBQ10* or *TA3*) and is displayed relative to

1042 WT. Each data point represents a biological replicate and is the average of three
1043 technical replicates, bars represent the mean and error bars the mean±s.e.m.
1044 Plants were grown in SD conditions.
1045
1046 **Figure S4. RY sites are not required for the temporal decline of *MIR156C***
1047 (A) qRT-PCR analyses of gene expression in shoot apices with LP ≥ 1mm removed
1048 at 1 and 2 weeks. Bars represent the average of three technical replicates for a
1049 single biological replicate of pooled T1 plants, at least 15 independent T1 plants
1050 were pooled for each sample. *qm = mir156a mir156c mir157a mir157c quadruple*
1051 *mutant, tm = mir156a mir157a mir157c triple mutant*. Plants were grown in SD
1052 conditions.
1053
1054 **Figure S5. *VAL* genes do not regulate *SPL9* chromatin state**
1055 (A, B) Temporal analysis of histone modification scalculated by ChIP-qPCR. Each data
1056 point represents a biological replicate and is the average of three technical
1057 replicates. Lines represent the mean and bars represent the mean±s.e.m., (A)
1058 H3K2me3 values are relative to H3 and normalised to *STM* as an internal control.
1059 (B) H2AK119ub values are relative to input and normalised to *ACT7* as an
1060 internal control. Plants were grown in SD conditions.
1061
1062 **Figure S6. *VAL1* expression is dependent on genetic elements in the coding**
1063 **sequence of the gene**

1064 (A) Torpedo-stage embryos of two-independent homozygous transgenic lines each
1065 expressing a transcriptional (top panel) or translational (bottom panel) *VAL1-*
1066 *GUS* reporter construct.
1067 (B) Seedlings at 3 DAG. Each number designates an independent homozygous
1068 transgenic line. Arrow heads point to initiating lateral root primordia. All plants
1069 were grown in LD.
1070

1071 **Figure S7. Proteomic changes during vegetative development**

1072 (A,B) The 50 proteins with the strongest increasing or decreasing trend score during
1073 vegetative development in the experimental sample only (see Methods for
1074 details). (A) GO terms enriched within the 50 proteins that have the strongest
1075 increasing or decreasing trend score. (G) Interaction networks for each set of 50
1076 proteins, the darker the color the stronger the increasing (red) or decreasing
1077 (blue) trend score.
1078

1079 **Table S1. Primer sequences**

1080 This table includes all the primer sequences used in this study.
1081

1082 **Table S2. Proteins detected by mass spectrometry following anti-HA**
1083 **immunoprecipitation**

1084 Related to Figure S6.
1085 This table includes the raw mass spectrometry results and data processing for IP-
1086 samples.

1087

1088 **Table S3. Total proteome changes during vegetative development**

1089 Related to Figure S6.

1090 This table includes the raw mass spectrometry results and data processing for total

1091 proteome samples.

1092

1093 **REFERENCES**

1094 Aguilan, J.T., Kulej, K., and Sidoli, S. (2020). Guide for protein fold change and p-value
1095 calculation for non-experts in proteomics. Mol. Omics *16*, 573–582.

1096 Baile, F., Merini, W., Hidalgo, I., and Calonje, M. (2020). Dissection of PRC1 and PRC2
1097 recruitment in Arabidopsis connects EAR repressome to PRC2 anchoring. BioRxiv
1098 2020.08.28.271999.

1099 Beydler, B., Osadchuk, K., Cheng, C.-L., Manak, J.R., and Irish, E.E. (2016). The Juvenile Phase of
1100 Maize Sees Upregulation of Stress-Response Genes and Is Extended by Exogenous Jasmonic
1101 Acid. Plant Physiol. *171*, 2648–2658.

1102 Bouveret, R., Schönrock, N., Gruissem, W., and Hennig, L. (2006). Regulation of flowering time
1103 by *Arabidopsis MSI1*. Development *133*, 1693–1702.

1104 Bratzel, F., López-Torrejón, G., Koch, M., Del Pozo, J.C., and Calonje, M. (2010). Keeping Cell
1105 Identity in Arabidopsis Requires PRC1 RING-Finger Homologs that Catalyze H2A
1106 Monoubiquitination. Current Biology *20*, 1853–1859.

1107 Calonje, M. (2014). PRC1 Marks the Difference in Plant PcG Repression. Molecular Plant *7*, 459–
1108 471.

1109 Carbonero, P., Iglesias-Fernández, R., and Vicente-Carbajosa, J. (2017). The AFL subfamily of B3
1110 transcription factors: evolution and function in angiosperm seeds. Journal of Experimental
1111 Botany *68*, 871–880.

1112 Chanvivattana, Y., Bishopp, A., Schubert, D., Stock, C., Moon, Y.-H., Sung, Z.R., and Goodrich, J.
1113 (2004). Interaction of Polycomb-group proteins controlling flowering in *Arabidopsis*.
1114 Development *131*, 5263–5276.

1115 Chen, N., Veerappan, V., Abdelmageed, H., Kang, M., and Allen, R.D. (2018). HSI2/VAL1 Silences
1116 *AGL15* to Regulate the Developmental Transition from Seed Maturation to Vegetative Growth
1117 in Arabidopsis. Plant Cell *30*, 600–619.

1118 Chen, N., Wang, H., Abdelmageed, H., Veerappan, V., Tadege, M., and Allen, R.D. (2020).
1119 HSI2/VAL1 and HSL1/VAL2 function redundantly to repress DOG1 expression in Arabidopsis
1120 seeds and seedlings. New Phytologist *227*, 840–856.

1121 Chhun, T., Chong, S.Y., Park, B.S., Wong, E.C.C., Yin, J.-L., Kim, M., and Chua, N.-H. (2016). HSI2
1122 Repressor Recruits MED13 and HDA6 to Down-Regulate Seed Maturation Gene Expression
1123 Directly During Arabidopsis Early Seedling Growth. Plant and Cell Physiology *57*, 1689–1706.

1124 Choi, K., Kim, J., Muller, S.Y., Oh, M., Underwood, C., Henderson, I., and Lee, I. (2016).
1125 Regulation of microRNA-mediated developmental changes by the SWR1 chromatin remodeling
1126 complex. Plant Physiol *171*, 1128–1143.

1127 Cui, Y., Cheng, J., Ruan, S., Qi, P., Liu, W., Bian, H., Ye, L., Zhang, Y., Hu, J., Dong, G., et al. (2020).
1128 The heterochronic gene Oryza sativa LIKE HETEROCHROMATIN PROTEIN 1 modulates
1129 miR156b/c/i/e levels. Journal of Integrative Plant Biology *62*, 1839–1852.

1130 Engler, C., Youles, M., Gruetzner, R., Ehnert, T.M., Werner, S., Jones, J.D., Patron, N.J., and
1131 Marillonnet, S. (2014). A golden gate modular cloning toolbox for plants. ACS Synth. Biol. *3*,
1132 839–843.

1133 Fouracre, J.P., and Poethig, R.S. (2019). Role for the shoot apical meristem in the specification
1134 of juvenile leaf identity in *Arabidopsis*. Proc Natl Acad Sci USA *116*, 10168–10177.

1135 German, M.A., Pillay, M., Jeong, D.-H., Hetawal, A., Luo, S., Janardhanan, P., Kannan, V.,
1136 Rymarquis, L.A., Nobuta, K., German, R., et al. (2008). Global identification of microRNA–target
1137 RNA pairs by parallel analysis of RNA ends. Nature Biotechnology *26*, 941–946.

1138 Goodrich, J., Puangsomlee, P., Martin, M., Long, D., Meyerowitz, E.M., and Coupland, G. (1997).
1139 A Polycomb-group gene regulates homeotic gene expression in Arabidopsis. Nature *386*, 44–51.

1140 Gou, J.Y., Felippes, F.F., Liu, C.J., Weigel, D., and Wang, J.W. (2011). Negative regulation of
1141 anthocyanin biosynthesis in Arabidopsis by a miR156-targeted SPL transcription factor. Plant
1142 Cell *23*, 1512–1522.

1143 Guo, C., Xu, Y., Shi, M., Lai, Y., Wu, X., Wang, H., Zhu, Z., Poethig, R.S., and Wu, G. (2017).
1144 Repression of miR156 by miR159 regulates the timing of the juvenile-to-adult transition in
1145 *Arabidopsis*. Plant Cell *29*, 1293–1304.

1146 Guo, X., Hou, X., Fang, J., Wei, P., Xu, B., Chen, M., Feng, Y., and Chu, C. (2013). The rice
1147 *GERMINATION DEFECTIVE 1*, encoding a B3 domain transcriptional repressor, regulates seed
1148 germination and seedling development by integrating GA and carbohydrate metabolism. The
1149 Plant Journal *75*, 403–416.

1150 He, J., Xu, M., Willmann, M.R., McCormick, K., Hu, T., Yang, L., Starker, C.G., Voytas, D.F.,
1151 Meyers, B.C., and Poethig, R.S. (2018). Threshold-dependent repression of *SPL* gene expression

1152 by miR156/miR157 controls vegetative phase change in *Arabidopsis thaliana*. PLoS Genet. *14*,
1153 e1007337.

1154 Huijser, P., and Schmid, M. (2011). The control of developmental phase transitions in plants.
1155 Development *138*, 4117–4129.

1156 Jang, I.-C., Chung, P.J., Hemmes, H., Jung, C., and Chua, N.-H. (2011). Rapid and Reversible Light-
1157 Mediated Chromatin Modifications of Arabidopsis *Phytochrome A* Locus. Plant Cell *23*, 459–
1158 470.

1159 Jing, Y., Guo, Q., and Lin, R. (2019). The B3-Domain Transcription Factor VAL1 Regulates the
1160 Floral Transition by Repressing *FLOWERING LOCUS T*. Plant Physiol. *181*, 236–248.

1161 Kagaya, Y., Ohmiya, K., and Hattori, T. (1999). RAV1, a novel DNA-binding protein, binds to
1162 bipartite recognition sequence through two distinct DNA-binding domains uniquely found in
1163 higher plants. Nucleic Acids Research *27*, 470–478.

1164 Kim, K.-C., Lai, Z., Fan, B., and Chen, Z. (2008). *Arabidopsis* WRKY38 and WRKY62 Transcription
1165 Factors Interact with Histone Deacetylase 19 in Basal Defense. Plant Cell *20*, 2357–2371.

1166 Lawrence, E.H., Springer, C.J., Helliker, B.R., and Poethig, R.S. (2020). MicroRNA156-mediated
1167 changes in leaf composition lead to altered photosynthetic traits during vegetative phase
1168 change. New Phytologist.

1169 Leichty, A.R., and Poethig, R.S. (2019). Development and evolution of age-dependent defenses
1170 in ant-acacias. Proc Natl Acad Sci USA *116*, 15596–15601.

1171 Li, J., Wang, Z., Hu, Y., Cao, Y., and Ma, L. (2017). Polycomb Group Proteins RING1A and RING1B
1172 Regulate the Vegetative Phase Transition in Arabidopsis. Frontiers in Plant Science *8*, 867.

1173 Lopez-Vernaza, M., Yang, S., Müller, R., Thorpe, F., de Leau, E., and Goodrich, J. (2012).
1174 Antagonistic Roles of SEPALLATA3, FT and FLC Genes as Targets of the Polycomb Group Gene
1175 CURLY LEAF. PLOS ONE *7*, e30715.

1176 Mao, Y.-B., Liu, Y.-Q., Chen, D.-Y., Chen, F.-Y., Fang, X., Hong, G.-J., Wang, L.-J., Wang, J.-W., and
1177 Chen, X.-Y. (2017). Jasmonate response decay and defense metabolite accumulation
1178 contributes to age-regulated dynamics of plant insect resistance. Nature Communications *8*,
1179 13925.

1180 Molitor, A.M., Bu, Z., Yu, Y., and Shen, W.-H. (2014). Arabidopsis AL PHD-PRC1 Complexes
1181 Promote Seed Germination through H3K4me3-to-H3K27me3 Chromatin State Switch in
1182 Repression of Seed Developmental Genes. PLOS Genetics *10*, e1004091.

1183 Ossowski, S., Schneeberger, K., Clark, R.M., Lanz, C., Warthmann, N., and Weigel, D. (2008).
1184 Sequencing of natural strains of Arabidopsis thaliana with short reads. Genome Res *18*, 2024–
1185 2033.

1186 Pico, S., Ortiz-Marchena, M.I., Merini, W., and Calonje, M. (2015). Deciphering the role of
1187 Polycomb Repressive Complex 1 (PRC1) variants in regulating the acquisition of flowering
1188 competence in Arabidopsis. Plant Physiology *168*, 1286–1297.

1189 Qüesta, J.I., Song, J., Geraldo, N., An, H., and Dean, C. (2016). *Arabidopsis* transcriptional
1190 repressor VAL1 triggers Polycomb silencing at *FLC* during vernalization. Science *353*, 485–488.

1191 Ronemus, M., Vaughn, M.W., and Martienssen, R.A. (2006). MicroRNA-Targeted and Small
1192 Interfering RNA–Mediated mRNA Degradation Is Regulated by Argonaute, Dicer, and RNA-
1193 Dependent RNA Polymerase in *Arabidopsis*. Plant Cell *18*, 1559–1574.

1194 RStudio Team (2020). RStudio: Integrated Development Environment for R (Boston, MA:
1195 RStudio, PBC).

1196 Sasnauskas, G., Kauneckaitė, K., and Siksnys, V. (2018). Structural basis of DNA target
1197 recognition by the B3 domain of Arabidopsis epigenome reader VAL1. Nucleic Acids Research
1198 *46*, 4316–4324.

1199 Schindelin, J., Arganda-Carreras, I., Frise, E., Kaynig, V., Longair, M., Pietzsch, T., Preibisch, S.,
1200 Rueden, C., Saalfeld, S., Schmid, B., et al. (2012). Fiji: an open-source platform for biological-
1201 image analysis. Nature Methods *9*, 676–682.

1202 Schneeberger, K., Ossowski, S., Lanz, C., Juul, T., Petersen, A.H., Nielsen, K.L., Jorgensen, J.E.,
1203 Weigel, D., and Andersen, S.U. (2009). SHOREmap: simultaneous mapping and mutation
1204 identification by deep sequencing. Nat Methods *6*, 550–551.

1205 Serivichyaswat, P., Ryu, H.S., Kim, W., Kim, S., Chung, K.S., Kim, J.J., and Ahn, J.H. (2015).
1206 Expression of the floral repressor miRNA156 is positively regulated by the AGAMOUS-like
1207 proteins AGL15 and AGL18. Mol Cells *38*, 259–266.

1208 Shannon, P., Markiel, A., Ozier, O., Baliga, N.S., Wang, J.T., Ramage, D., Amin, N., Schwikowski,
1209 B., and Ideker, T. (2003). Cytoscape: A Software Environment for Integrated Models of
1210 Biomolecular Interaction Networks. Genome Research *13*, 2498–2504.

1211 Suzuki, M., Kao, C.Y., and McCarty, D.R. (1997). The conserved B3 domain of VIVIPAROUS1 has a
1212 cooperative DNA binding activity. Plant Cell *9*, 799–807.

1213 Suzuki, M., Wang, H.H.-Y., and McCarty, D.R. (2007). Repression of the *LEAFY COTYLEDON 1/B3*
1214 Regulatory Network in Plant Embryo Development by *VP1/ABSCISIC ACID INSENSITIVE 3-LIKE* B3
1215 Genes. Plant Physiol. *143*, 902–911.

1216 Telfer, A., Bollman, K.M., and Poethig, R.S. (1997). Phase change and the regulation of trichome
1217 distribution in *Arabidopsis thaliana*. Development *124*, 645–654.

1218 Tian, R., Wang, F., Zheng, Q., Niza, V.M.A.G.E., Downie, A.B., and Perry, S.E. (2020). Direct and
1219 indirect targets of the arabidopsis seed transcription factor ABSCISIC ACID INSENSITIVE3. The
1220 Plant Journal *103*, 1679–1694.

1221 Tsukagoshi, H., Morikami, A., and Nakamura, K. (2007). Two B3 domain transcriptional
1222 repressors prevent sugar-inducible expression of seed maturation genes in *Arabidopsis*
1223 seedlings. Proc Natl Acad Sci USA *104*, 2543–2547.

1224 Veerappan, V., Wang, J., Kang, M., Lee, J., Tang, Y., Jha, A.K., Shi, H., Palanivelu, R., and Allen,
1225 R.D. (2012). A novel HSI2 mutation in Arabidopsis affects the PHD-like domain and leads to
1226 derepression of seed-specific gene expression. Planta *236*, 1–17.

1227 Wang, F., and Perry, S.E. (2013). Identification of direct targets of FUSCA3, a key regulator of
1228 Arabidopsis seed development. Plant Physiology *161*, 1251–1264.

1229 Wang, L., Zhou, C.-M., Mai, Y.-X., Li, L.-Z., Gao, J., Shang, G.-D., Lian, H., Han, L., Zhang, T.-Q.,
1230 Tang, H.-B., et al. (2019). A spatiotemporally regulated transcriptional complex underlies
1231 heteroblastic development of leaf hairs in Arabidopsis thaliana. The EMBO Journal *38*, e100063.

1232 Weber, E., Engler, C., Gruetzner, R., Werner, S., and Marillonnet, S. (2011). A Modular Cloning
1233 System for Standardized Assembly of Multigene Constructs. PLOS ONE *6*, e16765.

1234 Wei, Q., Ma, C., Xu, Y., Wang, T., Chen, Y., Lü, J., Zhang, L., Jiang, C.-Z., Hong, B., and Gao, J.
1235 (2017). Control of chrysanthemum flowering through integration with an aging pathway.
1236 Nature Communications *8*, 829.

1237 Werner, S., Engler, C., Weber, E., Gruetzner, R., and Marillonnet, S. (2012). Fast track assembly
1238 of multigene constructs using Golden Gate cloning and the MoClo system. Bioeng Bugs *3*, 38–
1239 43.

1240 Wu, G., and Poethig, R.S. (2006). Temporal regulation of shoot development in *Arabidopsis*
1241 *thaliana* by miR156 and its target *SPL3*. Development *133*, 3539–3547.

1242 Wu, G., Park, M.Y., Conway, S.R., Wang, J.W., Weigel, D., and Poethig, R.S. (2009). The
1243 sequential action of miR156 and miR172 regulates developmental timing in *Arabidopsis*. Cell
1244 *138*, 750–759.

1245 Wu, G., Rossidivito, G., Hu, T., Berlyand, Y., and Poethig, R.S. (2015). Traffic lines: new tools for
1246 genetic analysis in *Arabidopsis thaliana*. Genetics *200*, 35–45.

1247 Xie, Y., Zhang, Y., Han, J., Luo, J., Li, G., Huang, J., Wu, H., Tian, Q., Zhu, Q., Chen, Y., et al.
1248 (2018). The Intronic *cis* Element *SE1* Recruits *trans*-Acting Repressor Complexes to Repress the
1249 Expression of *ELONGATED UPPERMOST INTERNODE1* in Rice. Molecular Plant *11*, 720–735.

1250 Xu, M., Hu, T., Zhao, J., Park, M.Y., Earley, K.W., Wu, G., Yang, L., and Poethig, R.S. (2016a).
1251 Developmental functions of miR156-regulated *SQUAMOSA PROMOTER BINDING PROTEIN-LIKE*
1252 (*SPL*) genes in *Arabidopsis thaliana*. PLoS Genet. *12*, e1006263.

1253 Xu, M., Leichty, A.R., Hu, T., and Poethig, R.S. (2018). H2A.Z promotes the transcription of
1254 *MIR156A* and *MIR156C* in *Arabidopsis* by facilitating the deposition of H3K4me3. Development
1255 *145*, dev152868.

1256 Xu, M.L., Hu, T.Q., Smith, M.R., and Poethig, R.S. (2016b). Epigenetic regulation of vegetative
1257 phase change in *Arabidopsis*. Plant Cell *28*, 28–41.

1258 Xu, Y.M., Guo, C.K., Zhou, B.Y., Li, C.L., Wang, H.S., Zheng, B., Ding, H., Zhu, Z.J., Peragine, A.,
1259 Cui, Y.H., et al. (2016c). Regulation of vegetative phase change by SWI2/SNF2 chromatin
1260 remodeling ATPase BRAHMA. Plant Physiol *172*, 2416–2428.

1261 Yang, C., Bratzel, F., Hohmann, N., Koch, M., Turck, F., and Calonje, M. (2013a). VAL- and
1262 AtBMI1-Mediated H2Aub Initiate the Switch from Embryonic to Postgerminative Growth in
1263 Arabidopsis. Current Biology *23*, 1324–1329.

1264 Yang, H., Howard, M., and Dean, C. (2014). Antagonistic Roles for H3K36me3 and H3K27me3 in
1265 the Cold-Induced Epigenetic Switch at Arabidopsis FLC. Current Biology *24*, 1793–1797.

1266 Yang, L., Xu, M., Koo, Y., He, J., and Poethig, R.S. (2013b). Sugar promotes vegetative phase
1267 change in *Arabidopsis thaliana* by repressing the expression of *MIR156A* and *MIR156C*. Elife *2*,
1268 e00260.

1269 Yu, S., Cao, L., Zhou, C.M., Zhang, T.Q., Lian, H., Sun, Y., Wu, J.Q., Huang, J.R., Wang, G.D., and
1270 Wang, J.W. (2013). Sugar is an endogenous cue for juvenile-to-adult phase transition in plants.
1271 Elife *2*, e00269.

1272 Yuan, L., Song, X., Zhang, L., Yu, Y., Liang, Z., Lei, Y., Ruan, J., Tan, B., Liu, J., and Li, C. (2020). The
1273 transcriptional repressors VAL1 and VAL2 recruit PRC2 for genome-wide Polycomb silencing in
1274 Arabidopsis. Nucleic Acids Research.

1275 Yuan, W., Luo, X., Li, Z., Yang, W., Wang, Y., Liu, R., Du, J., and He, Y. (2016). A cis cold memory
1276 element and a trans epigenome reader mediate Polycomb silencing of FLC by vernalization in
1277 Arabidopsis. Nature Genetics *48*, 1527–1534.

1278 Zeng, X., Gao, Z., Jiang, C., Yang, Y., Liu, R., and He, Y. (2020). HISTONE DEACETYLASE 9
1279 Functions with Polycomb Silencing to Repress *FLOWERING LOCUS C* Expression. Plant Physiol.
1280 *182*, 555–565.

1281 Zhao, H., Lin, K., Ma, L., Chen, Q., Gan, S., and Li, G. (2020). Arabidopsis NUCLEAR FACTOR Y A8
1282 inhibits the juvenile-to-adult transition by activating transcription of MIR156s. Journal of
1283 Experimental Botany *71*, 4890–4902.

1284 Zhou, Y., Tan, B., Luo, M., Li, Y., Liu, C., Chen, C., Yu, C.-W., Yang, S., Dong, S., Ruan, J., et al.
1285 (2013). HISTONE DEACETYLASE19 interacts with HSL1 and participates in the repression of seed
1286 maturation genes in Arabidopsis seedlings. Plant Cell *25*, 134–148.

1287 Zhou, Y., Romero-Campero, F.J., Gómez-Zambrano, Á., Turck, F., and Calonje, M. (2017). H2A
1288 monoubiquitination in Arabidopsis thaliana is generally independent of LHP1 and PRC2 activity.
1289 Genome Biology *18*, 69.

1290

1291

1292

1293

1294

1295

1296

1297

1298

1299